Electronic Supplementary Material (ESI) for Soft Matter.
This journal is © The Royal Society of Chemistry 2018

Unravelling the 2D Self-Assembly of Fmoc-Dipeptides at Fluid Interfaces

Pablo Gómez-Argudo,[1] Rafael Contreras-Montoya,[2] Luis Álvarez de Cienfuegos,,[2] Juan M. Cuerva,[2] Manuel Cano,[1] David Alba-Molina,[1] María T. Martín-Romero,[1] Luis Camacho,[1] Juan J. Giner-Casares*,[1]*

[1]Departamento de Química Física y T. Aplicada, Instituto Universitario de Investigación en Química Fina y Nanoquímica IUIQFN, Facultad de Ciencias, Universidad de Córdoba, Campus de Rabanales, Ed. Marie Curie, E-14071 Córdoba, Spain
[2]Departamento de Química Orgánica, Facultad de Ciencias, Universidad de Granada, (UGR), C. U. Fuentenueva, Granada E-18071, Spain.

Experimental section

Materials. The initial 0.5 mM solutions of phenyl dipeptides were prepared in dichloromethane, while the rest of the dipeptides were in methanol. Solvents were used without further purification from Aldrich (Germany). Ultrapure water, produced by a Millipore Milli-Q unit, pre-treated by a Millipore reverse osmosis system (>18.2 MΩ cm), was used as subphase. The subphase temperature was 21 ºC with pH 2. The pH 2 subphase was prepared with Hydrochloric acid 37% PRS-Codex purchased from Panreac. All instruments for the study of the dipeptides at the air/liquid interface were located on tables with vibration isolation (antivibration system MOD-2 S, Accurion, Göttingen, Germany) in a large class 100 clean room. Fmoc-LG, Fmoc-AA, Fmoc-GG and Fmoc-FF were purchase from Bachem Co., Switzerland; Fmoc-Y and Fmoc-F were purchase from Sigma-Aldrich.

Surface pressure–area isotherms. Two different models of Nima troughs (Nima Technology, Coventry, England) were used in this work, both provided with a Wilhelmy type dynamometric system using a strip of filter paper: a NIMA 611D with one moving barrier for the measurement of the reflection spectra, and a NIMA 601, equipped with two symmetrical barriers to record BAM images. The layers of Fmoc-dipeptides were compressed at a speed of 0.03 nm^2 min^{-1} $molecule^{-1}$.

UV-vis reflection spectroscopy. UV–visible reflection spectra at normal incidence as the difference in reflectivity (ΔR) of the film-covered water surface and the bare surface were obtained with a Nanofilm Surface Analysis Spectrometer (Ref SPEC2, supplied by Accurion GmbH, Göttingen, Germany).

Brewster angle microscopy. Images of the film morphology were obtained by Brewster angle microscopy (BAM) with a I-Elli2000 (Accurion GmbH) using a Nd:YAG diode laser with wavelength 532 nm and 50 mW, which can be recorded with a lateral resolution

of 2 μm. The image processing procedure included a geometrical correction of the image, as well as a filtering operation to reduce interference fringes and noise. The measurement of thickness of the supramolecular structures was performed by ImageJ software.

Langmuir-Schaefer transferred films. The multilayers were transferred onto quartz substrates by sequential monolayer transfer. These monolayers were transferred by Langmuir-Schaefer, *i. e.*, by horizontal dipping at constant surface pressure. The transfer ratio was close to unity for all transfer processes.

UV-Visible absorption spectroscopy of films. The UV-vis spectra of the films were measured locating the substrate directly in the light path on a Cary 100 UV-Vis spectrophotometer.

UV-Visible absorption spectroscopy of solutions. UV-vis spectra of the Fmoc group and Fmoc-dipeptides in bulk solution were measured using an Analytik Jena SPECORD® 200 Plusand.

Circular dichroism (CD) spectroscopy of films. CD measurements were acquired using a UV-Vis Jasco J-1500 spectrophotometer. All spectra were recorded at room temperature. The spectra were measured in the wavelength interval from 190 to 350 nm with a 0.1 nm step resolution. The scanning rate was 15 nm/min with 2 s response time. The signal-to-noise ratio was improved by accumulating 3 scans for each CD spectrum. Data processing was carried out using the software package. The blank spectrum of the bare quartz substrate was subtracted.

Circular dichroism (CD) spectroscopy of the hydrogels. The CD spectra were recorded using an Olis DSM172 spectrofotometer with a xenon lamp of 150W. The hydrogels were gelated into a 0.1 mm quartz cell (Hellma 0.1 mm quartz Suprasil®). All of them were prepared at 2 $mg \cdot mL^{-1}$; Fmoc-CF hydrogel was prepared by solvent-switch with dimethylsulfoxide and water 5:95; Fmoc-MF and Fmoc-FF were prepared by pH-switch by addition of 2 molar equivalents of glucono-δ-lactone (GdL) to a basic peptide solution. Spectra were obtained from 190 to 350 nm with a 1 nm step and 0.1 s integration time per step at 25 ^{o}C, taking 20 averages.

Scanning Electron Microscopy (SEM). SEM images were obtained using an JEOL JSM 7800F with acceleration voltage from 0.5to 30 kv.

Raman spectroscopy. The spectra of Fmoc-CF were measured with a Raman microscope Renishaw InVia spectrophotometer, equipped with a Leica DM2500 M confocal microscope. Spectra were obtained by excitation with green laser light (532nm). The laser beam was focused on the specimen using the 100× lens, which was equivalent to sampling a theoretical spot of 2 μm. Reflected light was scattered through a diffraction slit of 1200 lines/mm and signals recorded by a CCD detector. Raman spectra were acquired over the wavenumber range 100–4000 cm−1, using an acquisition time of 20 s and 10 cumulative scans to improve the signal noise. The laser power used for spectral acquisition is from 50% of the maximum level (100 mW) a preheating of 20s was carried out avoiding combustion of the compound. The spectra were corrected by the elimination of the cosmic rays, the background subtraction and the signal corresponding to the bare glass.

Nuclear Magnetic Resonance (NMR). NMR Spectra were recorded were recorded on NMR 300 MHz spectrometer (Variant), and 500 MHz spectrometer (Bruker). Chemical

shifts (δ), referenced to the residual protonated solvent as an internal standard, are quoted in ppm. Coupling constants (J) are reported in Hz.

High Resolution Mass Spectrometry. Mass spectra were recorded using an Xevo G2-XS QTof (Waters, USA) mass spectrometer.

Dynamic Light Scattering (DLS). DLS experiments were performed using a Zetasizer Nano ZS Instrument (Malvern Instruments Ltd., Malvern, UK). The DLS measurements were performed at 25◦Cusing the red line (wavelength, λ = 632 nm) of a He-Ne laser in a quasi-backscattering configuration (scattering angle, θ = 173º). Previously to each measurement, the solutions were filtered in a cleanroom using a 0.45 μm Nylon membrane (Millex®, USA) to remove the dust particles. The filtered samples were transferred to a quartz measurement cell (Hellma®6030-OG Model). In DLS experiments the normalized intensity or second-order autocorrelation function was measured, $g^{(2)}(q,t)$, that is related to the electric field or first-order autocorrelation function, $g^{(1)}(q,t)$, through the Siegert relationship,

$$g^{(2)}(q,t) - 1 = \beta \left| g^{(1)}(q,t) \right|^2$$

where t is the time, $q = (4\pi n/\lambda) \sin(\theta/2)$ is the wavevector, and n the solution refractive index. β is an optical coherence factor and is generally found to be close to 1, except for cases in which the scattered intensity is low. Either because of the low size of the scatterers, low concentration or poor refractive index contrast between the scatterers and the solvent.

Section SI1. Solid phase protocol for the synthesis of Fmoc-CF, Fmoc-MF and Fmoc-RF.

All materials were of analytical grade and used without further purification. Fmoc-Phe-OH, Fmoc-Met-OH, Fmoc-Cys(Trt)-OH, Fmoc-Arg(Pbf)-OH, 4-dimethylaminopyridine (DMAP), trifluoroacetic acid (TFA) and triisopropylsilane (TIS) were purchase from Sigma-Aldrich, USA. 1-hydroxybenzotriazole (HOBt) and N,N'-diisopropylcarbodiimide (DIC) were purchase from FluoroChem, UK.

Step 1 – solid phase peptide coupling conditions used for the first coupling between p-alkoxybenzyl alcohol resin (Wang resin) and Fmoc-L-phenylalanine (Fmoc-Phe-OH):

Dry *p*-alkoxybenzyl alcohol resin (Wang resin) was placed in a round bottom flask under inert atmosphere. The resin was then swollen in dry dichloromethane (DCM) (10 mL per gram of resin). In another flask under inert atmosphere, Fmoc-Phe-OH (5 equiv) and HOBt (5 equiv) were dissolved in the minimum amount of dry N,N-dimethylformamide (DMF). Immediately after, DIC (5 equiv) was added and the mixture was stirred for 15 min before addition to the resin. After that, DMAP (0.01 equiv) solved in dry DMF was added to the reaction mixture. The mixture was agitated overnight at room temperature to effect coupling. To acetylate the resin hydroxyl free groups, pyridine (2 equiv) and acetic anhydride (2 equiv) were added to the suspension. The mixture was agitated for 15 min and the resin was washed with DMF (x5), DCM (x5) and diethyl ether (x2).

Step 2 – *N*-terminal Fmoc removal:

Fmoc removal was performed using 20% piperidine in DMF with two sequential treatments of 20 min. The resin was then filtered and washed with DMF (x5), DCM (x5) and diethyl ether (x2).

Step 3 – coupling of the second Fmoc-aminocid derivative:

The resin previously functionalized with phenylalanine was swollen in DMF. Then, Fmoc protected aminoacids (Fmoc-Cys(Trt)-OH, Fmoc-Met-OH or Fmoc-Arg(Pbf)-OH) (3.5 equiv) and HOBt (5 equiv) were dissolved in DMF. DIC (5 equiv) was added and the mixture and was stirred for 15 min. This mixture was added to the resin and was agitated for 2 h at 60 ºC to effect coupling. The resin was washed with DMF (x5), DCM (x5) and diethyl ether (x2). To test the efficiency of the coupling reaction, a qualitative Ninhydrin Test was carried-out after each coupling.[1]

Step 4 – cleavage of peptides from resin and removal of acid labile protecting groups:

Dry functionalized resin was suspended in 20 mL per gram of resin of TFA/water/1,2-ethanedithiol/TIS (92.5/2.5/2.5/2.5) and agitated for 2 h. The TFA solution was filtered, vacuum concentrated and added to cold (4 ºC) mixture of diethyl ether and hexane (2:1) in a centrifuge tube. The resulting precipitate was collected by centrifugation and washed with the mixture of diethyl ether and hexane (x3).

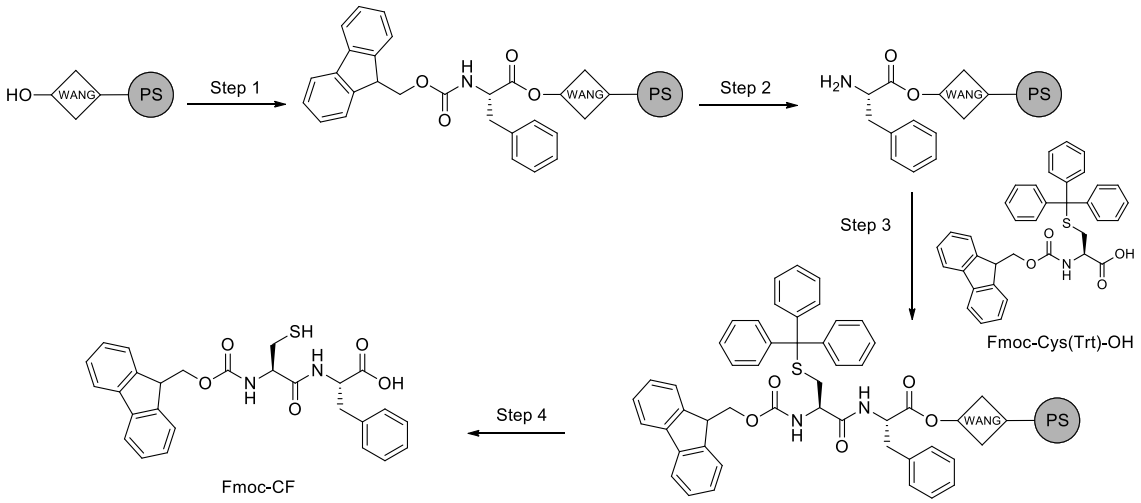

Figure SI1.1. **Synthetic scheme and NMR spectra of Fmoc-CF:**

Fmoc-CF: ^{1}H NMR (500 MHz, DMSO-d_6) δ 8.20 (s, 1H), 7.89 (d, J = 7.5 Hz, 2H), 7.73 (dd, J = 7.6, 3.8 Hz, 2H), 7.50 (d, J = 8.4 Hz, 1H), 7.41 (td, J = 7.5, 1.1 Hz, 2H), 7.35 – 7.30 (m, 2H), 7.25-7.00 (m, 5H), 6.67 (d, J = 8.4, 1H), 4.5-4.35 (m, 1H), 4.34 – 4.19 (m, 2H), 4.13 (s, 1H), 4.03 (s, 1H), 3.06 (dd, J = 14.0, 5.1 Hz, 1H), 2.98 – 2.84 (m, 1H), 2.81-2.70 (m, 1H), 2.67 – 2.56 (m, 1H). ^{13}C NMR (126 MHz, DMSO-d_6) δ 173.16, 170.04, 155.87, 143.83, 143.73, 140.68, 137.31, 129.95, 129.11, 128.21, 128.12, 127.62, 127.07, 126.40, 125.30, 120.08, 65.76, 57.04, 53.50, 46.62, 36.53, 26.29. HRMS (ESI): m/z calculated for $C_{27}H_{26}N_2O_5NaS$ $[M+Na]^+$: 513.1460; found: 513.1458.

^{1}H-NMR of Fmoc-CF:

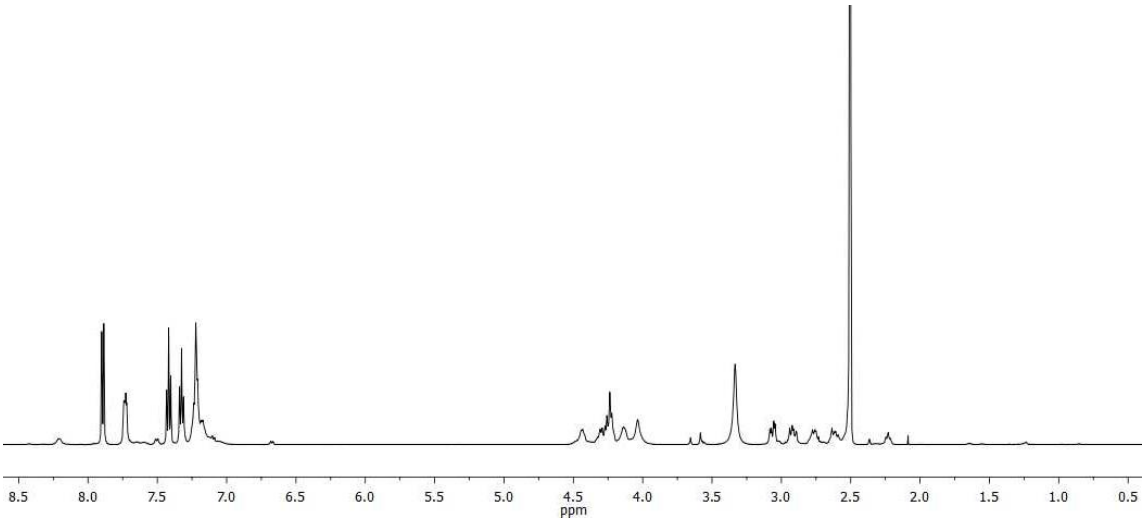

^{13}C-NMR of Fmoc-CF:

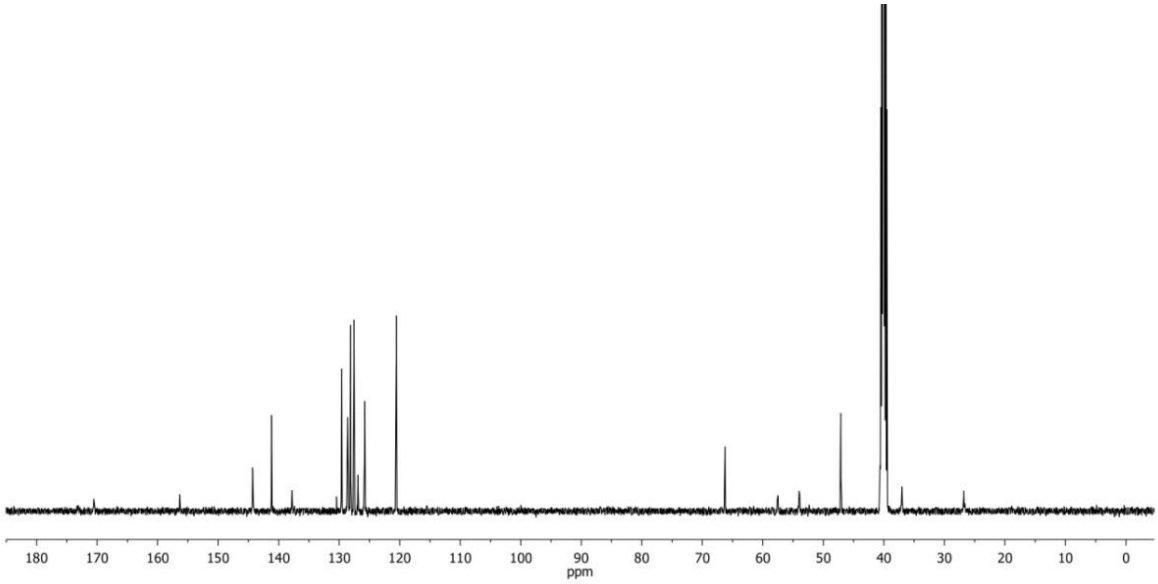

Figure SI1.2. **Synthetic scheme and NMR spectra of Fmoc-MF:**

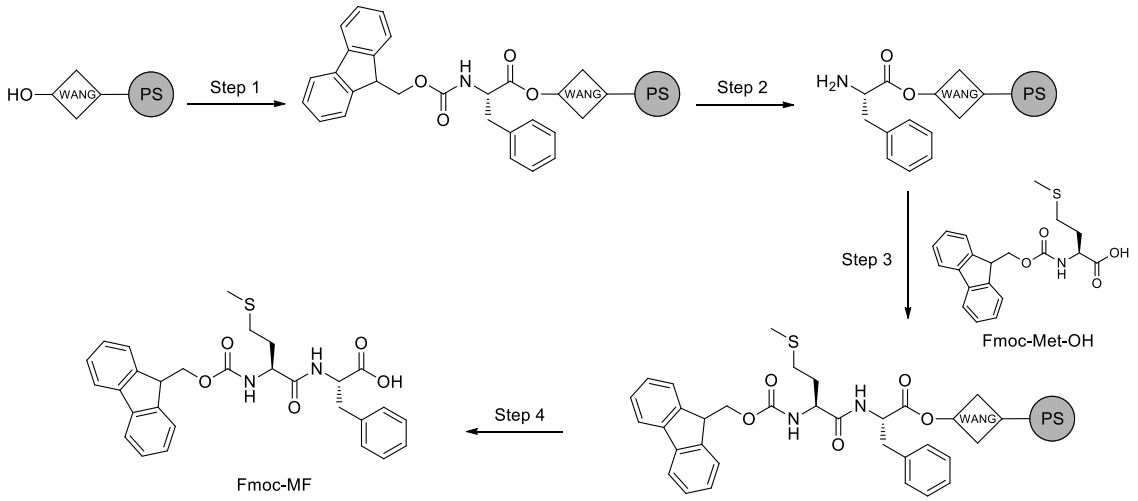

Fmoc-MF: ^{1}H NMR (300 MHz, $CDCl_3$-*d*) δ 7.76 (d, *J* = 6.9 Hz, 2H), 7.58 (d, *J* = 6.9 Hz, 2H), 7.40 (t, *J* = 7.0 Hz, 2H), 7.34 – 7.28 (m, 2H), 7.23 – 7.10 (m, 5H), 4.87 – 4.67 (m, 4H), 4.45 – 4.29 (m, 2H), 4.24 – 4.15 (m, 1H), 3.25 – 3.13 (m, 1H), 3.11 – 2.95 (m, 1H), 2.51 (d, *J* = 19.9 Hz, 2H), 2.09 – 1.84 (m, 5H). ^{13}C NMR (126 MHz, $CDCl_3$-*d*) δ 171.32, 156.29, 143.79, 141.46, 135.93, 129.48, 128.75, 127.95, 127.29, 127.26, 125.22, 125.17, 120.18, 67.35, 53.77, 53.57, 47.25, 37.57, 31.69, 30.03, 29.85, 15.24. HRMS (ESI): m/z calculated for $C_{29}H_{30}N_2O_5NaS$ $[M+Na]^+$: 541.1773; found: 541.1772.

^{1}H-NMR of Fmoc-MF:

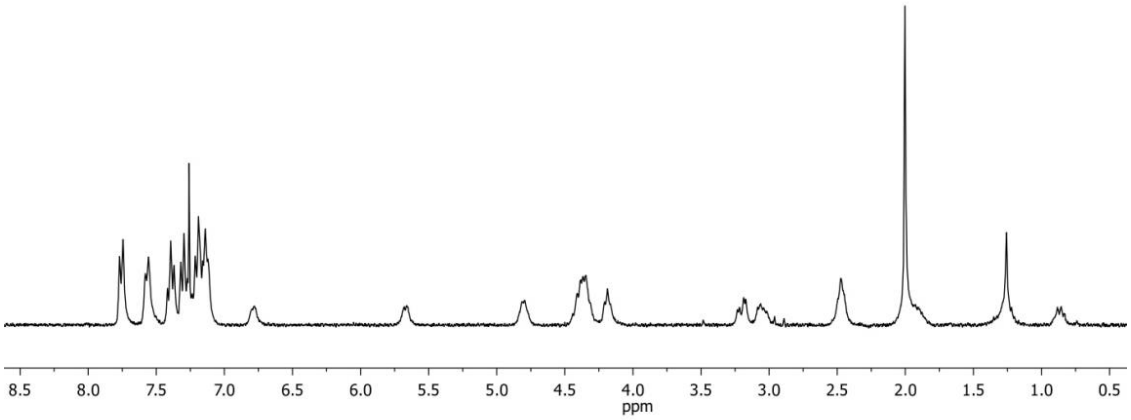

^{13}C-NMR of Fmoc-MF:

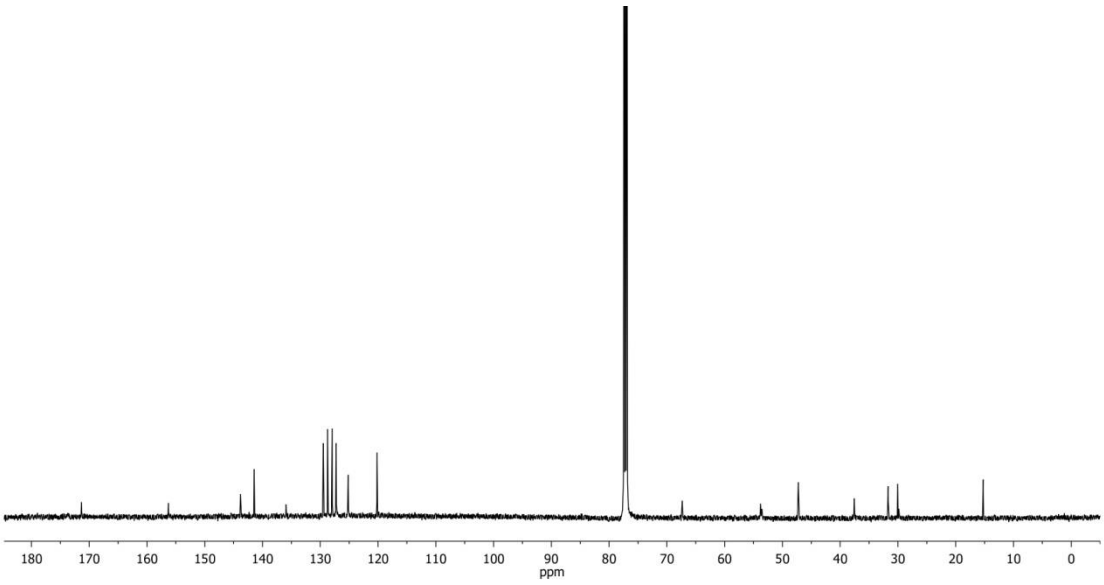

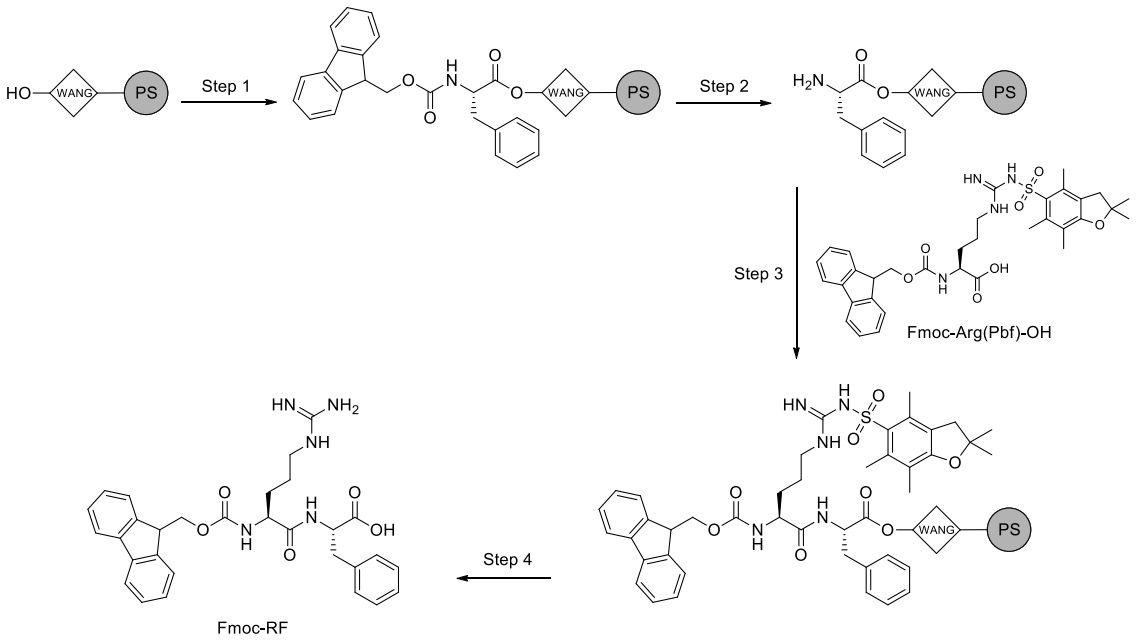

Figure SI1.3. **Synthetic scheme and NMR spectra of Fmoc-RF:**

Fmoc-RF: ^{1}H NMR (500 MHz, DMSO-d_6) δ 8.36 (d, J = 7.4 Hz), 8.11 (d, J = 7.8 Hz, 1H), 7.90 (d, J = 7.6 Hz, 2H), 7.72 (t, J = 8.1 Hz, 2H), 7.66 – 7.56 (m, 1H), 7.48 (d, J = 8.4 Hz, 1H), 7.42 (t, J = 7.5 Hz, 2H), 7.33 (t, J = 7.4 Hz, 2H), 7.29 – 7.13 (m, 5H), 4.52 – 4.39 (m, 1H), 4.32 – 4.18 (m, 3H), 4.03 (td, J = 8.4, 5.1 Hz, 1H), 3.57 (s, 1H), 3.12 – 2.99 (m, 3H), 2.93 (dd, J = 13.9, 8.6 Hz, 1H), 1.69-1.57 (m, 1H), 1.57-1.37 (m, 3H). ^{13}C NMR (126 MHz, DMSO-d_6) δ 172.85, 171.77, 171.49, 156.66, 155.81, 143.89, 143.71, 140.70, 137.48, 136.97, 129.16, 129.05, 128.21, 128.09, 127.65, 127.08, 126.55, 126.34, 125.31, 125.27, 120.11, 65.68, 54.05, 53.95, 53.60, 53.55, 51.83, 46.65, 40.38, 36.72, 36.57, 29.08, 24.97. HRMS (ESI): m/z calculated for $C_{27}H_{33}N_5O_5$ $[M+H]^+$: 544.2560; found: 544.2563.

^{1}H-NMR of Fmoc-RF:

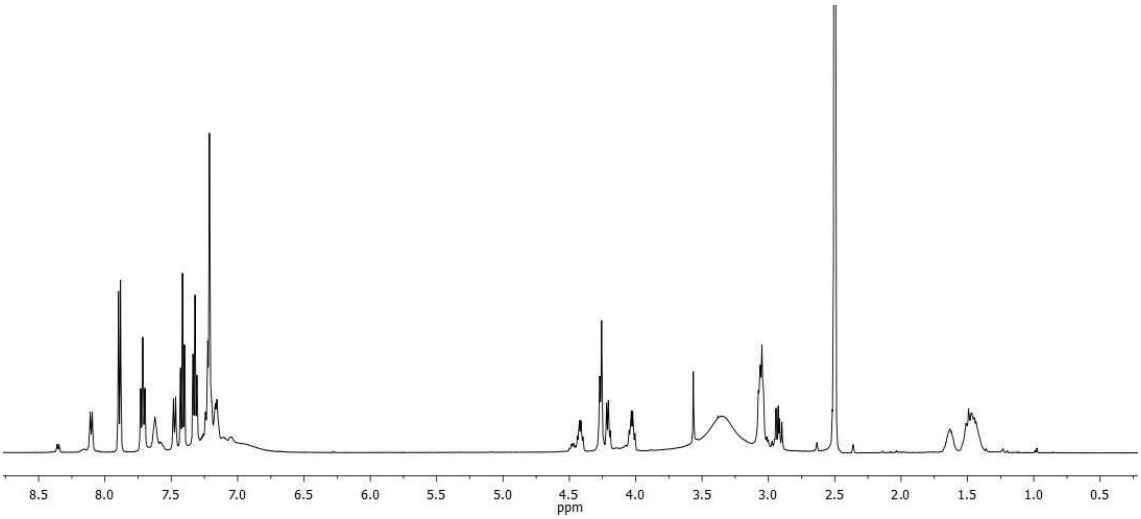

^{13}C-NMR of Fmoc-RF:

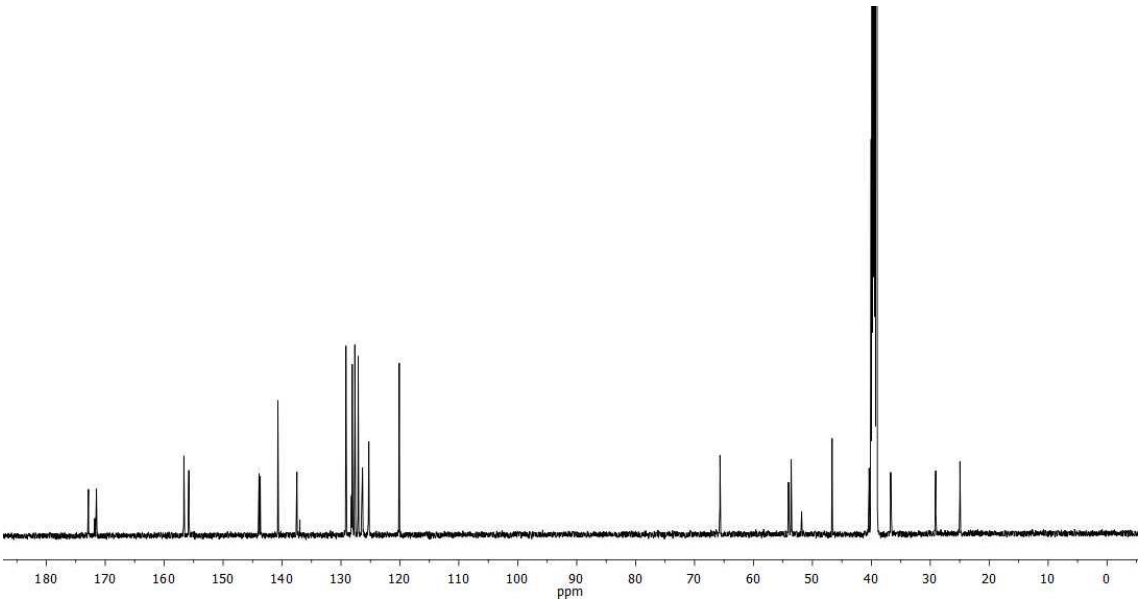

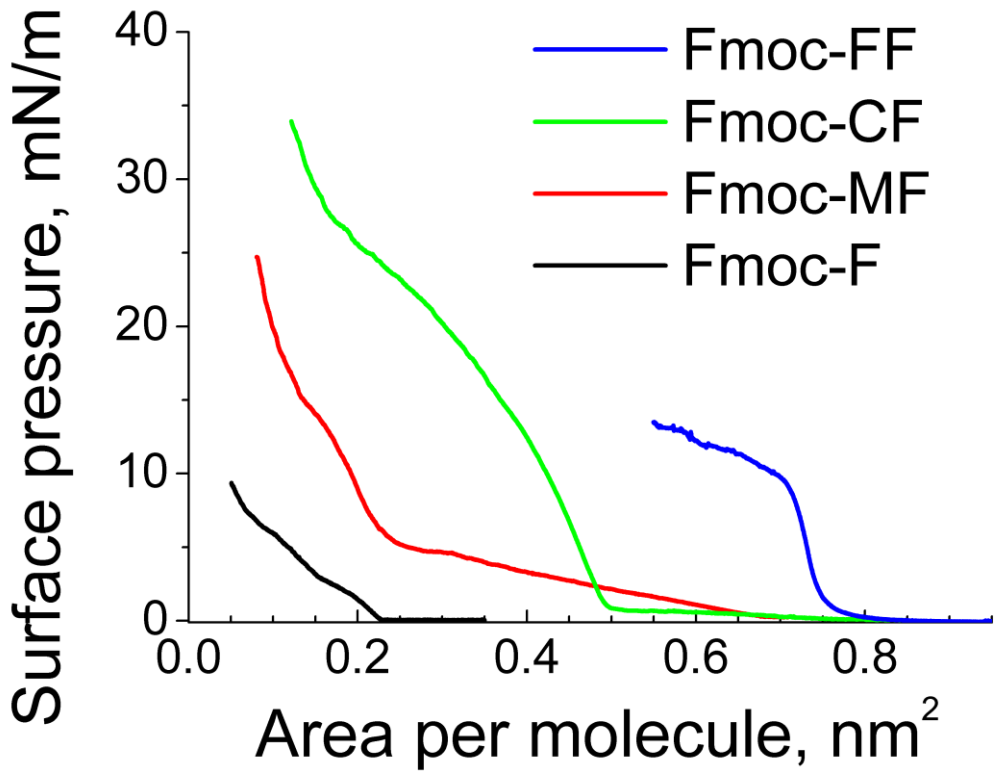

Figure SI2. Surface pressure – molecular area isotherms for the following Fmoc-dipeptides: Fmoc-F (red line), Fmoc-MF (green line), Fmoc-CF (black line), Fmoc-FF (black line). The subphase was in all cases a HCl solution adjusted to pH = 2.

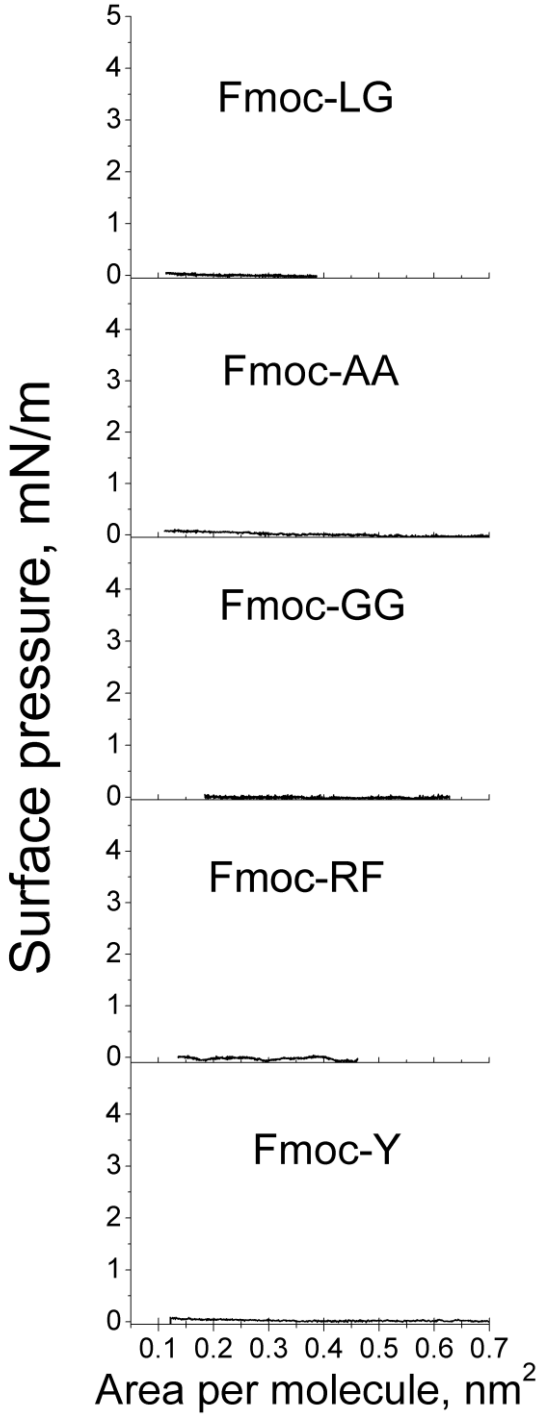

Figure SI3. Surface pressure – molecular area isotherms for the following Fmoc-dipeptides from top to bottom: Fmoc-LG, Fmoc-AA, Fmoc-GG, Fmoc-RF, Fmoc-Y. The subphase was in all cases a HCl solution adjusted to pH = 2.

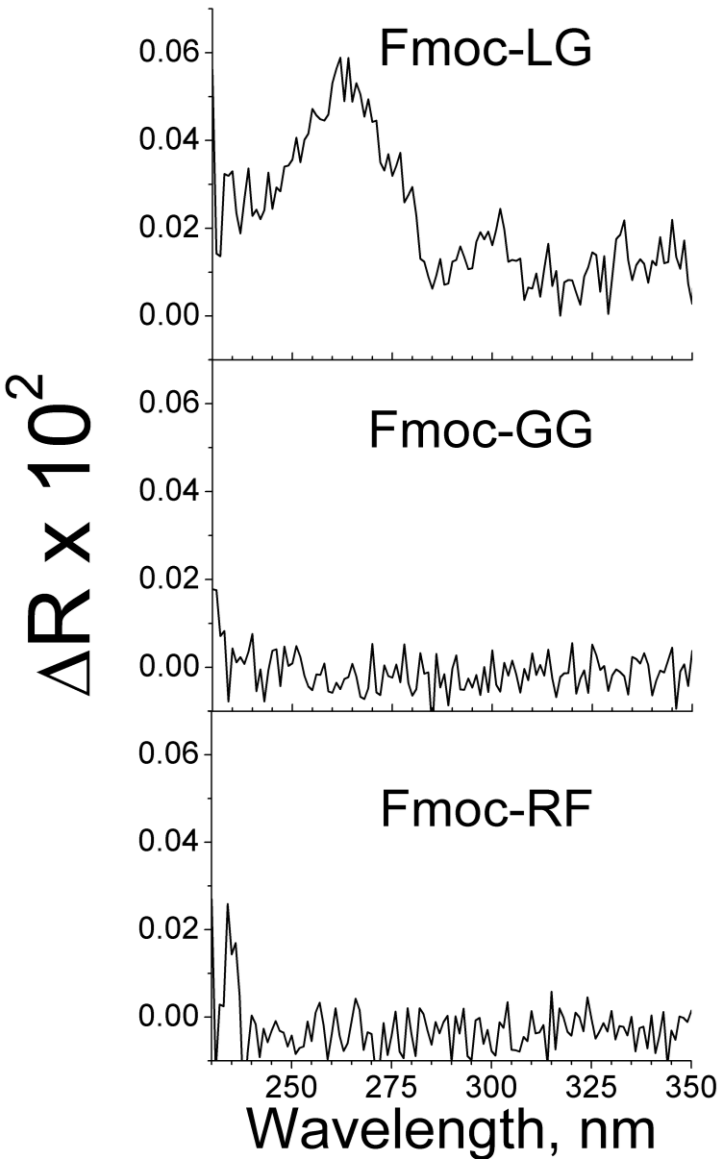

Figure SI4. UV-vis reflection spectra for the following Fmoc-dipeptides from top to bottom: Fmoc-LG (surface area of 0.11 nm^2/molecule), Fmoc-GG (surface area of 0.18 nm^2/molecule), Fmoc-RF (surface area of 0.27 nm^2/molecule). The subphase was in all cases a HCl solution adjusted to pH = 2.

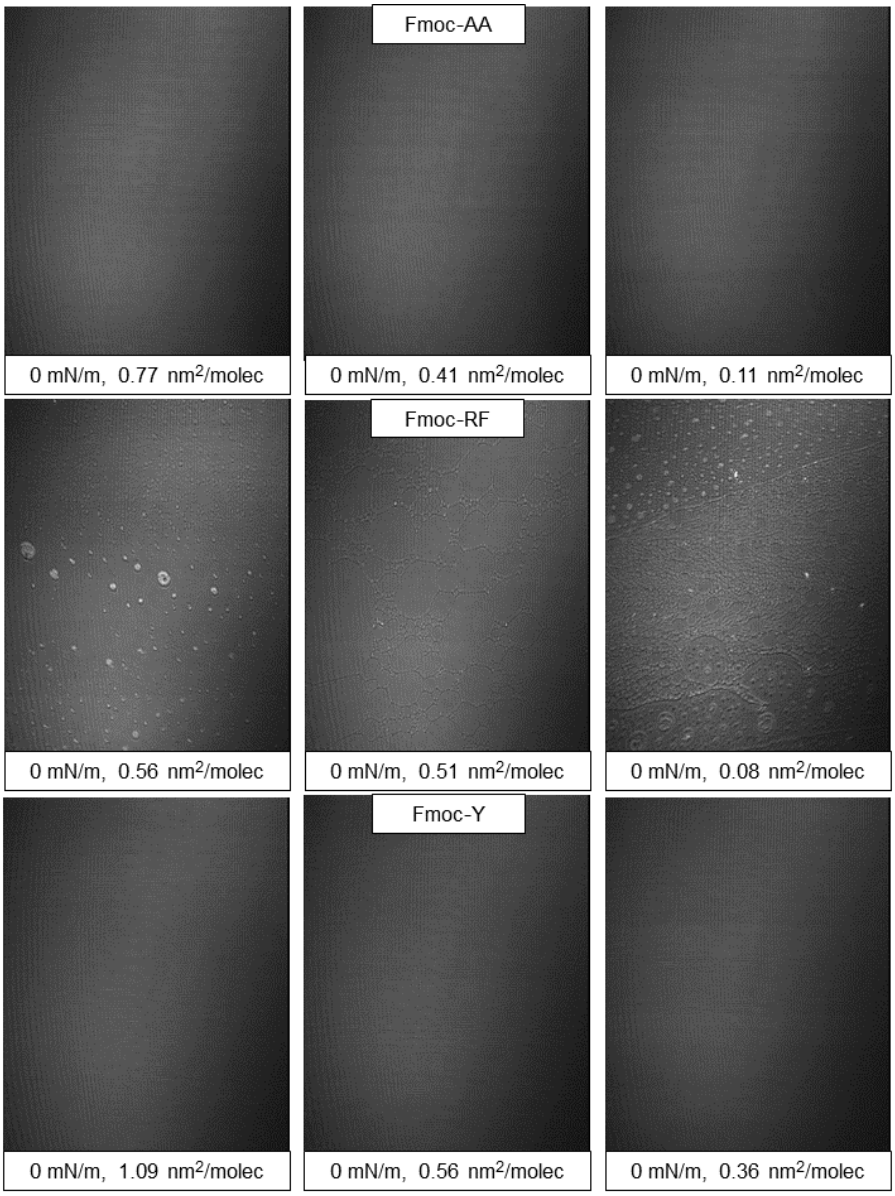

Figure SI5. Brewster angle microscopy pictures for the Fmoc-dipeptides at the air/water interface of Fmoc-AA, Fmoc-RF, Fmoc-Y, from top to bottom, respectively. The subphase was a HCl solution adjusted to pH = 2. The values of surface pressure and available surface area are included for each picture as inset. The width of each frame corresponds to 215 μm.

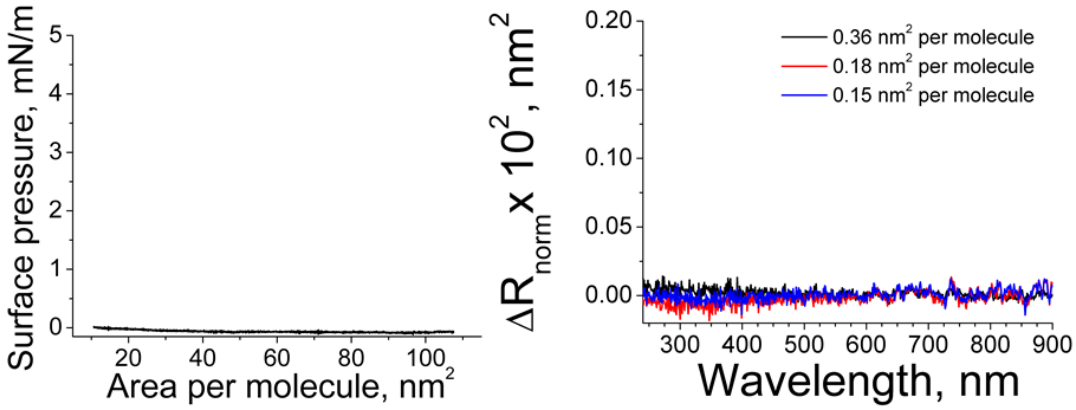

Figure SI6. Figure. Left) Surface pressure – molecular area isotherm of Fmoc-LG on a MilliQ water subphase. Right) UV-vis reflection spectra of Fmoc-LG at different values of available surface area per Fmoc-LG molecule as noted in the inset.

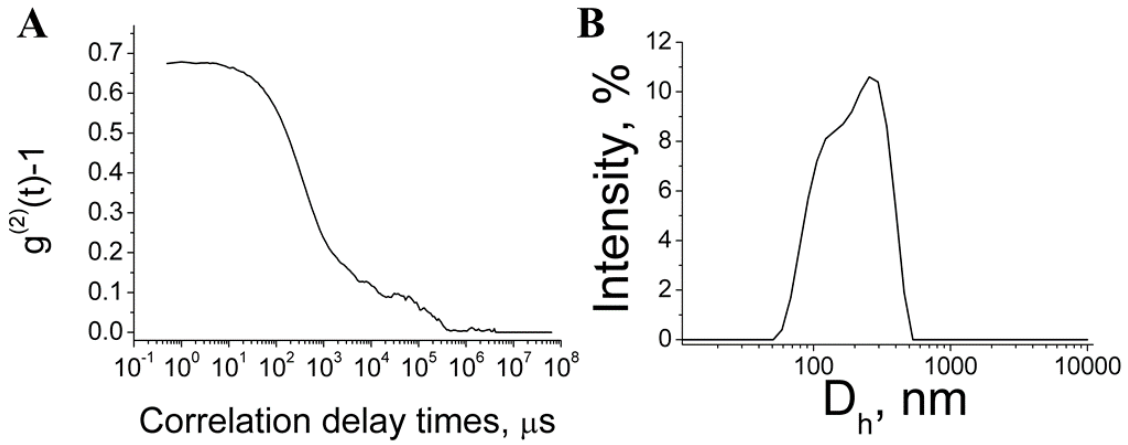

Figure SI7. A) DLS intensity auto-correlation function for bulk water after spreading of Fmoc-LG on the air/water interface. B) DLS spectrum of bulk water after spreading of Fmoc-LG on the air/water interface.

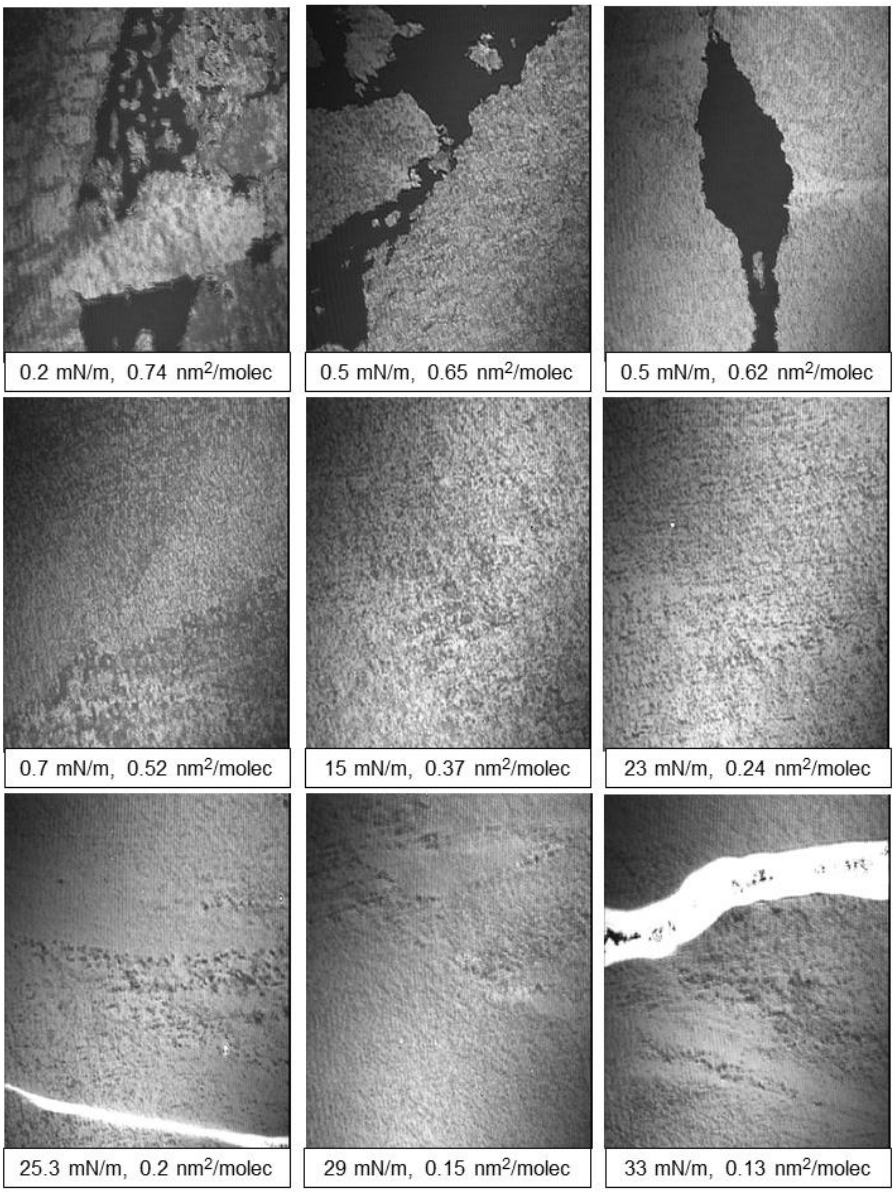

Figure SI8. Brewster angle microscopy pictures for the Fmoc-CF at the air/water interface. The subphase was a HCl solution adjusted to pH = 2. The values of surface pressure and available surface area are included for each picture as inset. The width of each frame corresponds to 215 μm.

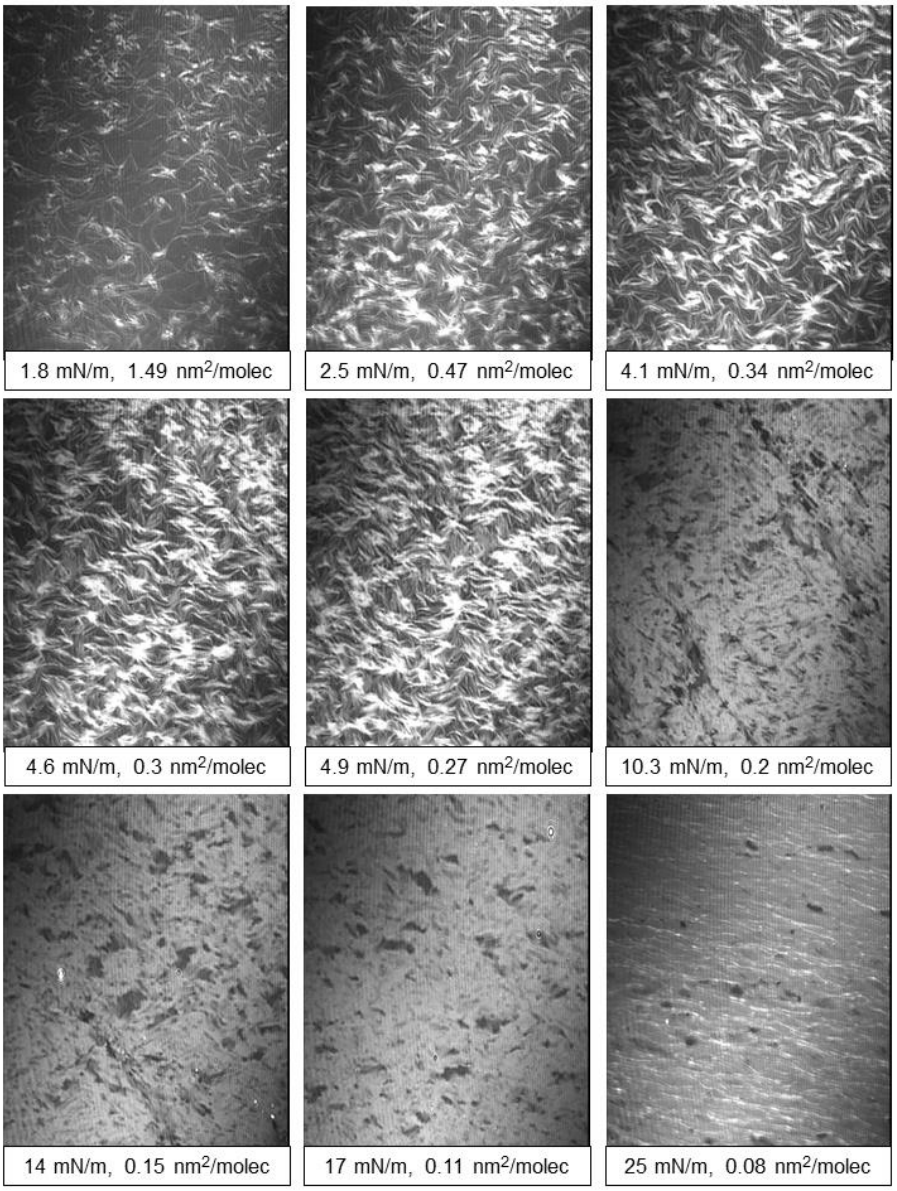

Figure SI9. Brewster angle microscopy pictures for the Fmoc-MF at the air/water interface. The subphase was a HCl solution adjusted to pH = 2. The values of surface pressure and available surface area are included for each picture as inset. The width of each frame corresponds to 215 μm.

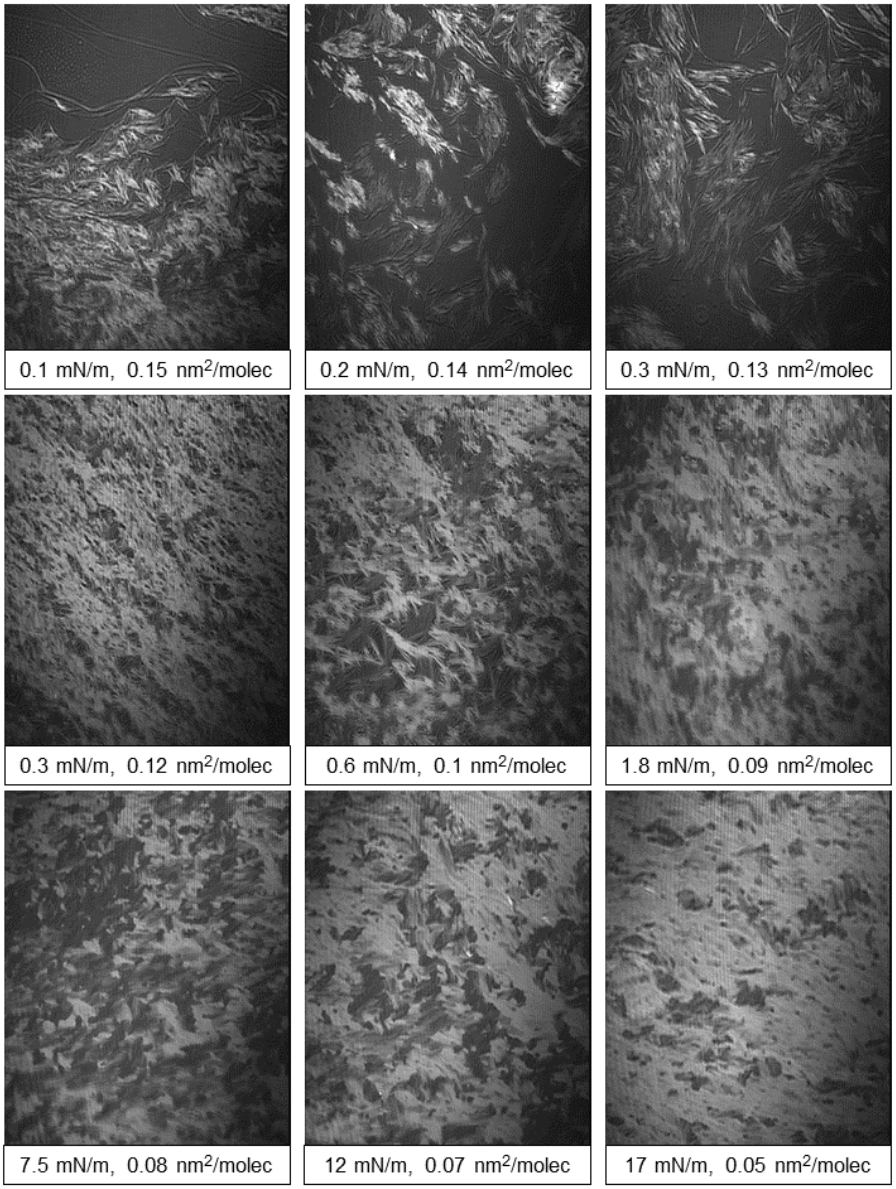

Figure SI10. Brewster angle microscopy pictures for the Fmoc-FF at the air/water interface. The subphase was a HCl solution adjusted to pH = 2. The values of surface pressure and available surface area are included for each picture as inset. The width of each frame corresponds to 215 μm.

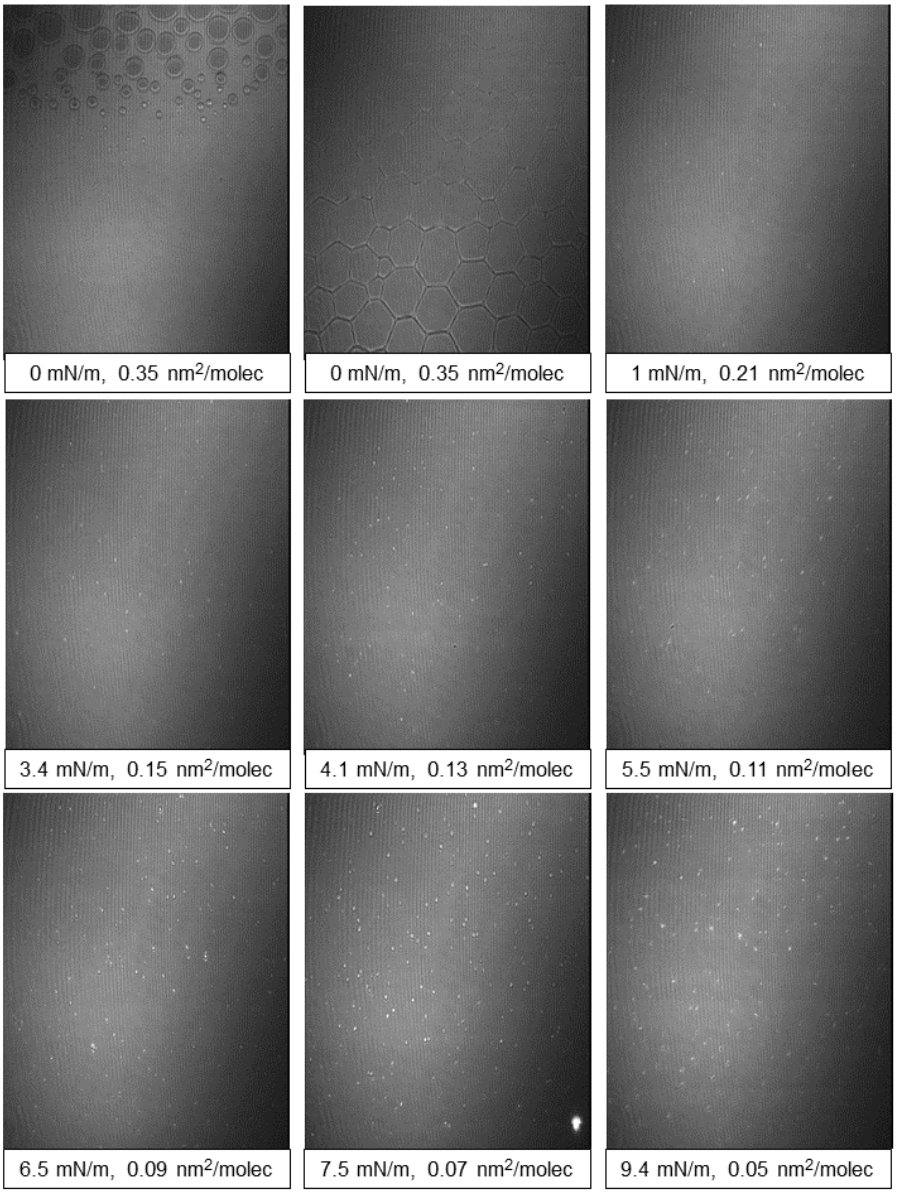

Figure SI11. Brewster angle microscopy pictures for the Fmoc-F at the air/water interface. The subphase was a HCl solution adjusted to pH = 2. The values of surface pressure and available surface area are included for each picture as inset. The width of each frame corresponds to 215 μm.

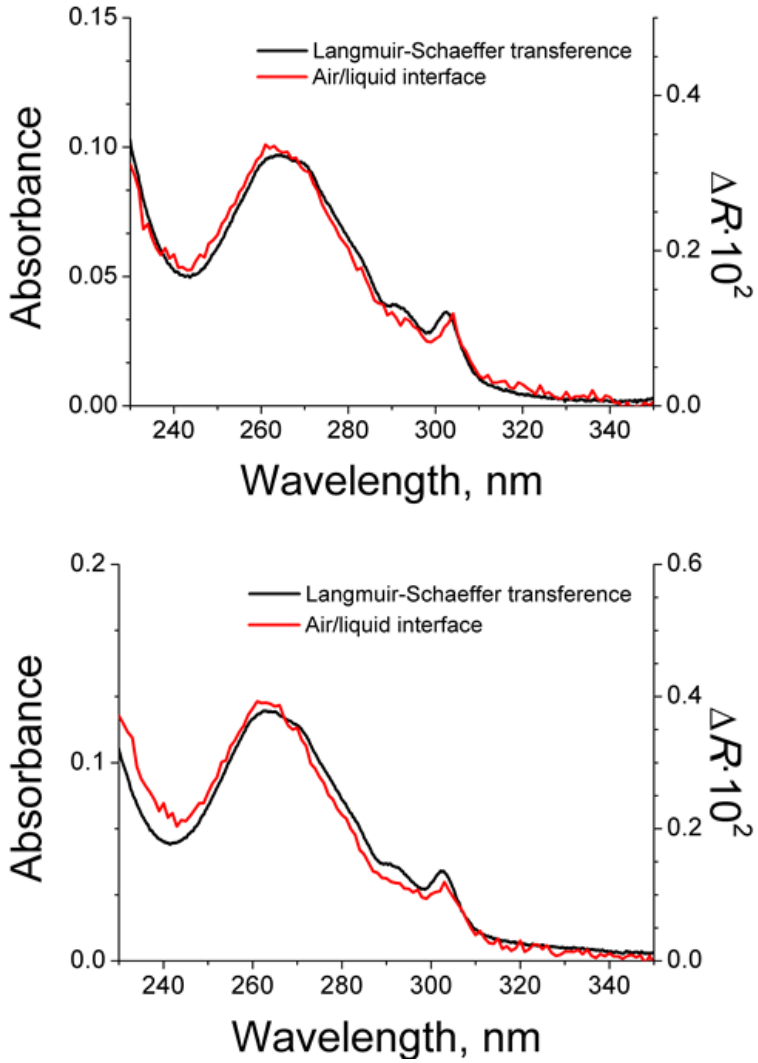

Figure SI12. Top) Bulk transmission UV-vis spectrum of Fmoc-FF transferred onto a quartz support (15 layers, π_{transf} = 8 mN/m, black line) and UV-vis reflection spectra (0.45 nm^2 per molecule, red line). Bottom) Bulk transmission UV-vis spectrum of Fmoc-MF transferred onto a quartz support (10 layers, π_{transf} = 20 mN/m, black line) and UV-vis reflection spectra (0.1 nm^2 per molecule, red line).

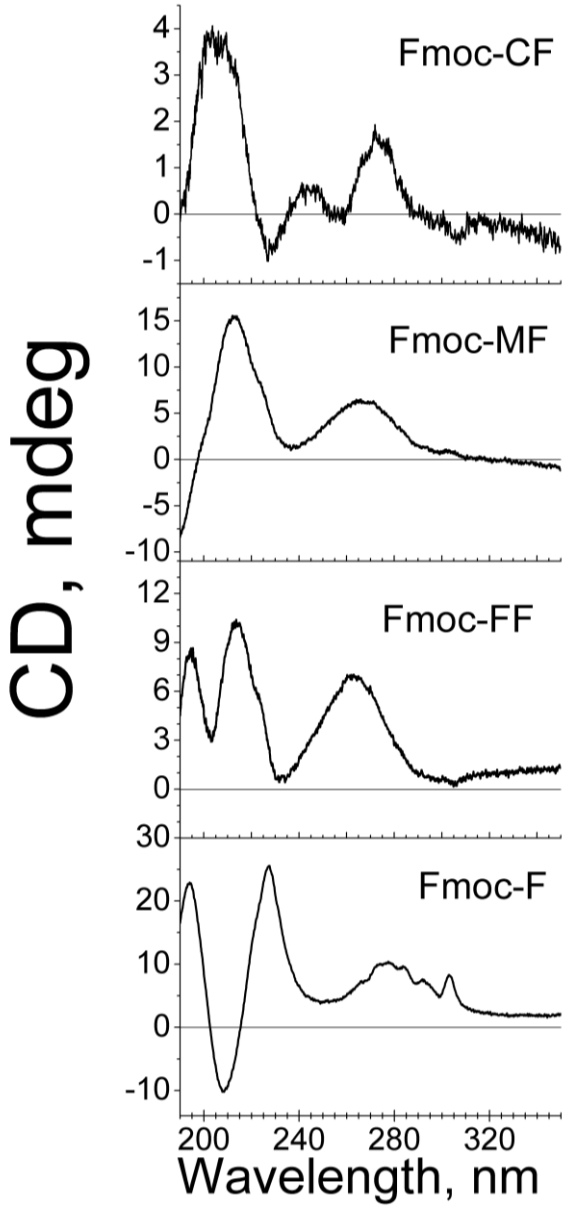

Figure SI13. Circular dichroism spectra for Langmuir-Schaeffer transferred Fmoc-dipeptides from the air/water interface onto quartz support. The transferred films are formed by the following Fmopc-dipeptides from top to bottom: Fmoc-CF (10 layers, π_{transf} = 30 mN/m), Fmoc-MF (10 layers, πt_{ransf} = 20 mN/m), Fmoc-FF (15 layers, π_{transf} = 8 mN/m), Fmoc-F (15 layers, π_{transf} = 8 mN/m).

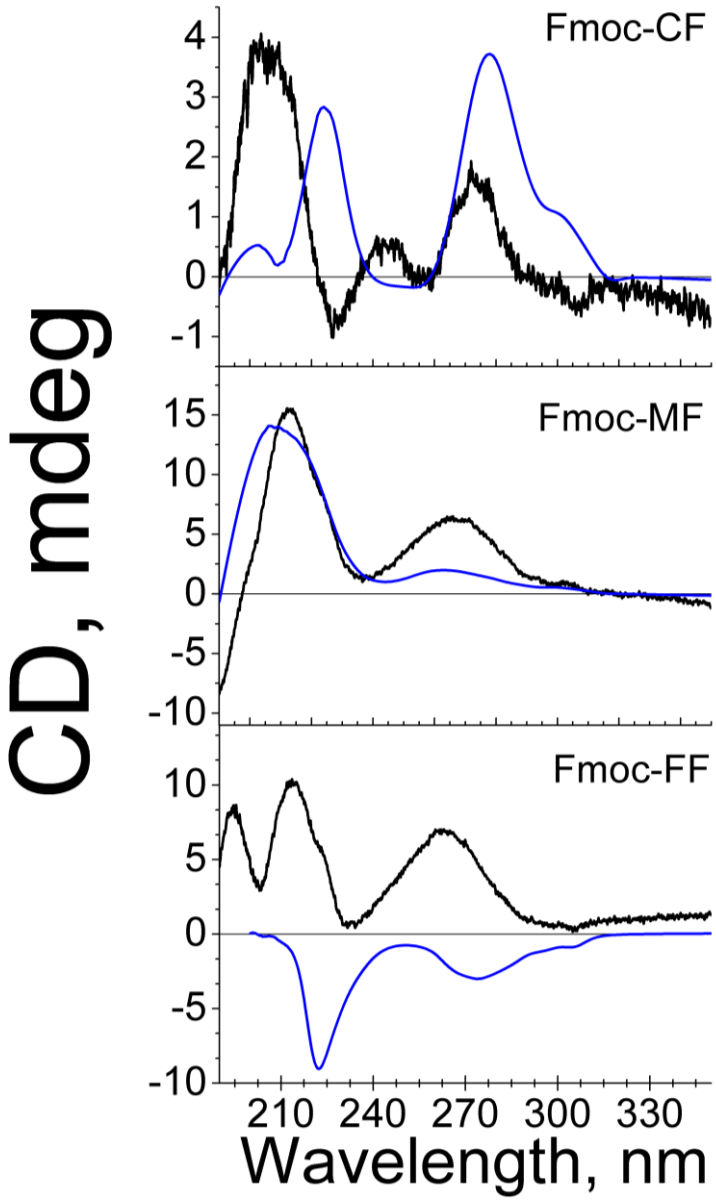

Figure SI14. Comparison of the circular dichroism spectra for Langmuir-Schaeffer transferred Fmoc-dipeptides from the air/water interface onto quartz support (black line) and bulk conditions forming hydrogel in solution (blue line). From top to bottom: Fmoc-CF, Fmoc-MF, Fmoc-FF.

Section SI15. Assessment of the UV-vis bands of the Fmoc group and the Fmoc-dipeptides in bulk solution.

The 9-fluorenylmethyloxycarbonyl (Fmoc) molecule shows three groups of bands in the UV-vis absorbance spectrum, see Figure SI15.1. A moderately intense bands are found at ca. 300 and 290 nm. A more complex region formed by the addition of several bands is found in the interval from 280 to 250 nm. A set of large signal are found at shorter wavelengths than 230 nm. The latter group is not relevant for the current discussion. The weak band observed at ca. 270 nm corresponds to the A_1 transition, polarized along the short axis of the Fmoc molecule. The other bands are ascribed to the B_2 transition, which are polarized along the long axis of the Fmoc molecule.[2] All the bands in the UV-vis transmission spectra of the Fmoc-dipeptides arise from the Fmoc group, as clearly seen in Figure SI13.1 and previously described for Fmoc-tetrapeptides.[3]

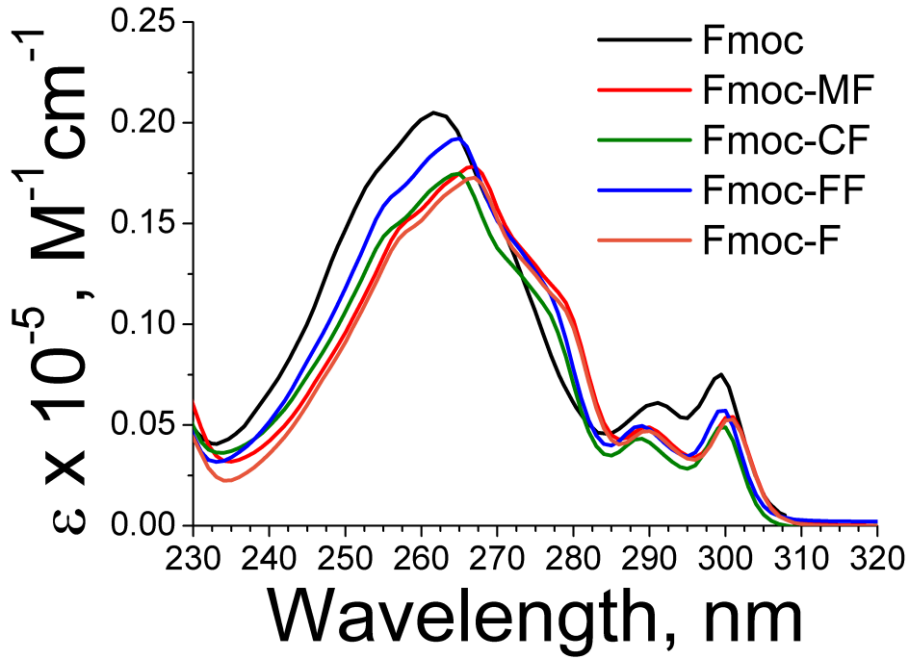

Figure SI15.1. UV-vis transmission spectra of the Fmoc group and Fmoc-dipeptides in bulk solution. The different derivatives of the Fmoc-dipeptides are noted in the inset.

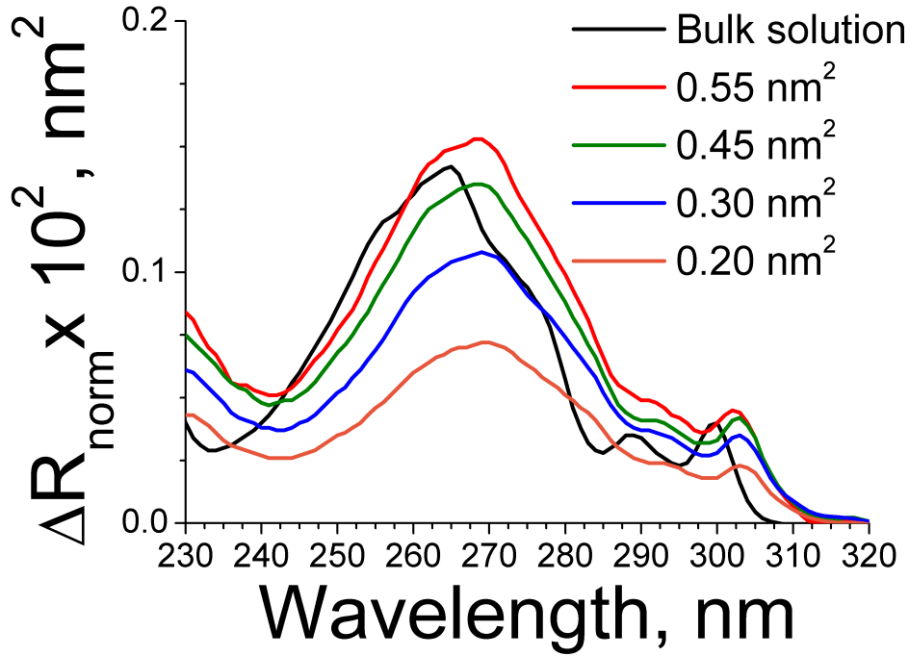

Figure SI15.2. UV-vis reflection spectra of the Fmoc-CF at the air/water interface. Surface area per Fmoc-CF molecule is noted in the inset. The UV-vis spectrum recorded in bulk solution is included as black line for comparison.

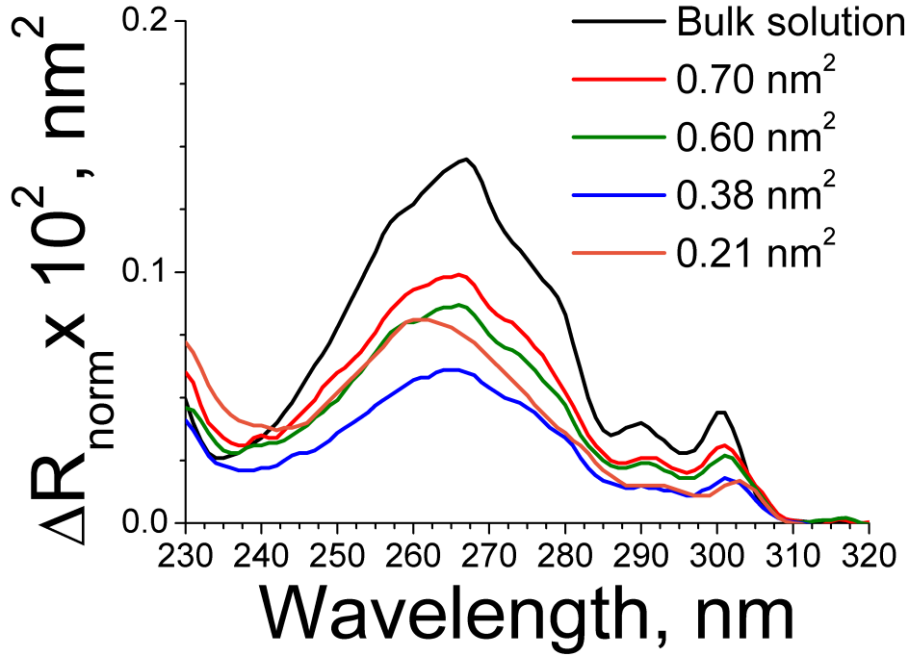

Figure SI15.3. UV-vis reflection spectra of the Fmoc-MF at the air/water interface. Surface area per Fmoc-MF molecule is noted in the inset. The intensity UV-vis reflection spectrum recorded at 0.21 nm^2 per Fmoc-dipeptide molecule has been increased by 1.5 for improving the clarity. The UV-vis spectrum recorded in bulk solution is included as black line for comparison.

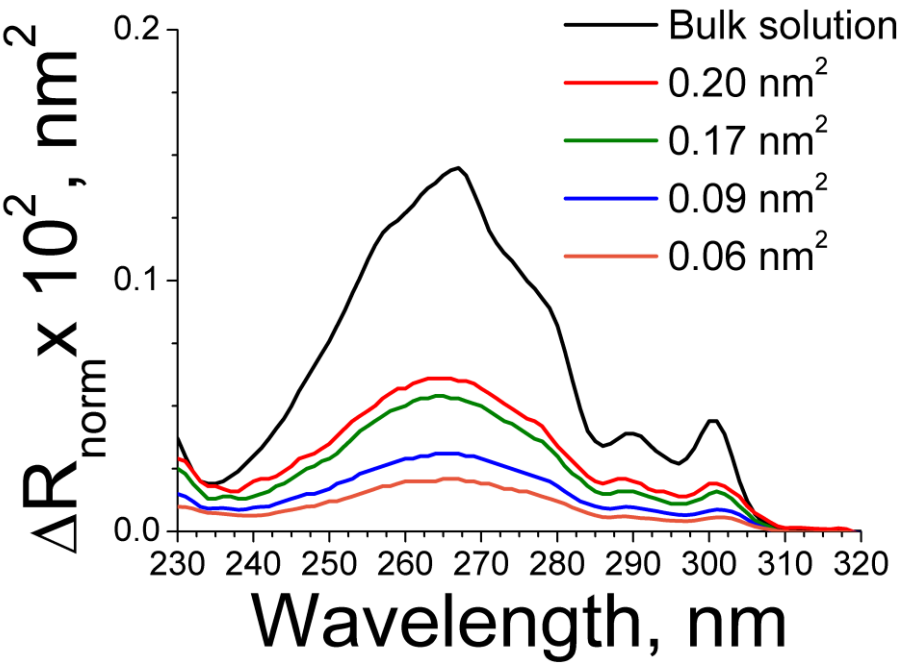

Figure SI15.4. UV-vis reflection spectra of the Fmoc-F at the air/water interface. Surface area per Fmoc-F molecule is noted in the inset. The UV-vis spectrum recorded in bulk solution is included as black line for comparison.

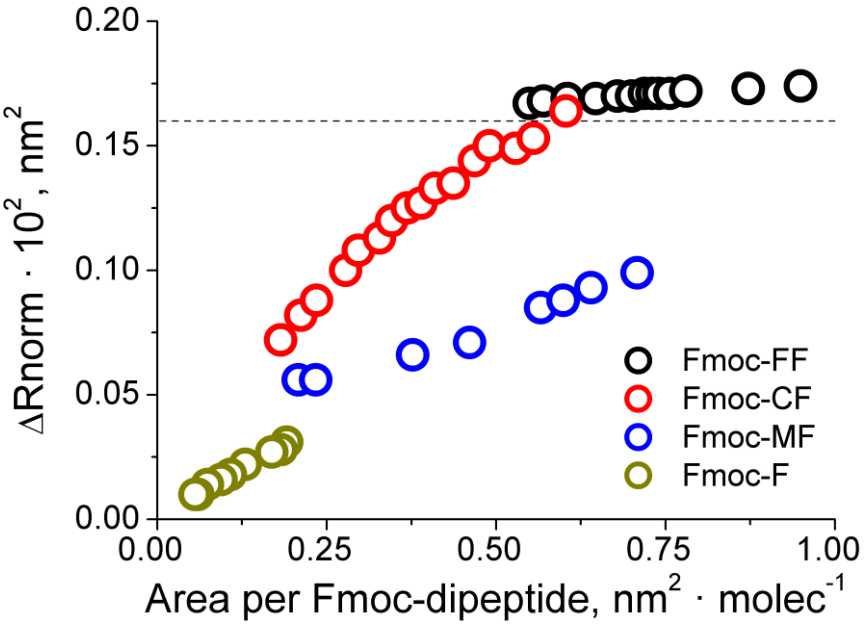

Figure SI15.5. Intensity values of the UV-vis reflection bands at 263-270 nm upon decrease of the available surface area for the supramolecular structures formed by the Fmoc-dipeptides. The different derivatives of the Fmoc-dipeptides are noted in the inset. The calculated maximum value of normalized UV-vis reflection is included as black line. ΔR_{norm} is ca. 0.16×10^{-2} nm^2 using $\varepsilon = 2\times 10^4$ mol·L^{-1}·cm^{-1} and $f_0 = 1.5$.

Section SI16. Molecular Dynamics Simulations of self-assembled supramolecular structures of Fmoc-FF at the air/water interface.

The self-assembly of Fmoc-dipeptides onto supramolecular structures is greatly affected by the pH. An antiparallel β sheet conformation as well as an antiparallel arrangement of the Fmoc groups is usually proposed as supramolecular structure of the Fmoc-dipeptides.[4,5] Nanostructured gels in bulk water can be obtained using Fmoc-Ala-Lac. Remarkably, Fmoc-Ala-Lac is not able to interact with other Fmoc-Ala-Lac molecules via β-sheet-like and amide-amide hydrogen bonding. Therefore, the formation of β-sheet-type supramolecular structures through H-bonding is not required to form supramolecular structures from short Fmoc-peptides. Instead, self-assembly driven by hydrophobic and aromatic interactions can form and stabilize self-assembled nanostructures of Fmoc-dipeptides.[6]

Molecular dynamics simulations were performed to attain insights on the supramolecular structure of the Fmoc-FF supramolecular structures self-assembled at the interface. Note that in view of the CD results the supramolecular arrangement might be different in supramolecular structures assembled at the air/water interface with respect to in bulk solution. The molecular dynamics simulations are aimed at modelling the initial stages of self-assembling of Fmoc-FF onto supramolecular structures rather than the compression stages of already formed supramolecular structures. The starting structure comprises an antiparallel β sheet conformation of the amide bonds and an antiparallel arrangement of the Fmoc groups. The longitudinal and transversal axes of the Fmoc group are placed parallel and slightly tilted with respect to the air/water interface, see Figure SI16.1.

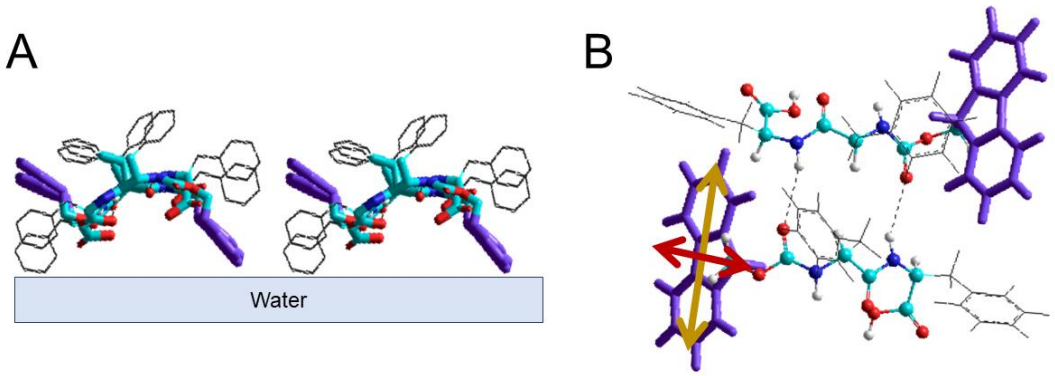

Figure SI16.1. Molecular sketch of the starting configuration for interacting Fmoc-FF molecules. A) side view and B) front view. The Fmoc groups are shown in purple for clarity. The yellow arrow indicates the longitudinal axis of the Fmoc group. The red arrow indicates the transversal axis of the Fmoc group.

A periodic box with the following dimension values was built: x = 40 Å, y = 45 Å, z = 110 Å, see Figure SI16.2. 2658 water molecules were placed in the central region of the box, *i. e.*, z-axis values between 35 and 75 Å. Density of bulk water is then close to 1 g/L. 16 Fmoc-FF molecules were placed in each water surface, thus amounting to a total of 32 Fmoc-FF molecules in the simulations. Two vacuum regions are included between the

two monolayers of Fmoc-FF to prevent interactions between the opposite monolayers, at z = 0-25 Å and z = 85-110 Å. This configuration allows simultaneously simulating two air/water interfaces. An average value of 1.12 nm^2 per Fmoc-FF dipeptide molecule is set. Such value of available surface area is intermediate between the two values of minimum surface area on the interface, *i. e.*, 1.48 and 0.86 nm^2.[7]

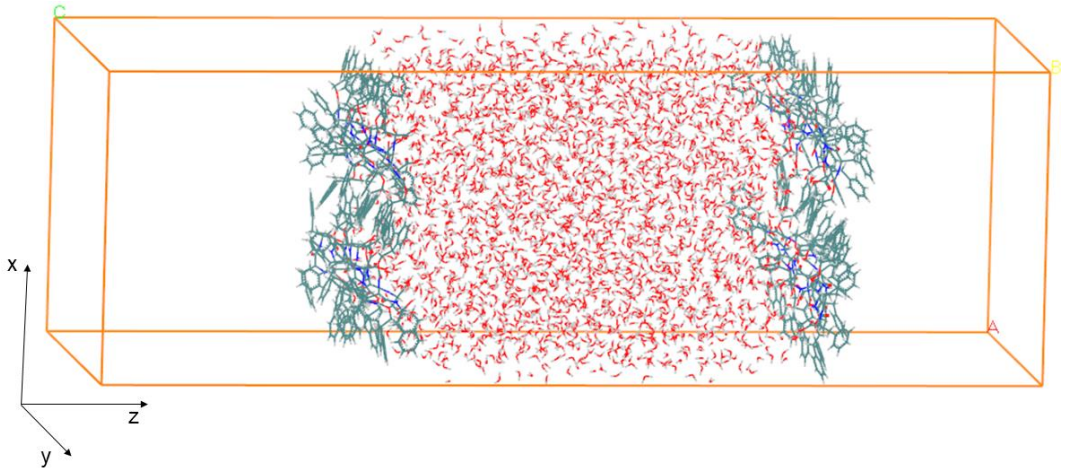

Figure SI16.2. Simulation box for the molecular dynamics simulations. Water molecules are depicted in red. Fmoc-FF molecules are depicted in blue and green. XYZ axes are included.

The geometry of the simulated box was optimized using the Universal Forcefield, assigning the charge values following the procedure described by Gasteiger and Marsili.[8,9] The following procedure was applied for four complete cycles: 1) Molecular Dynamics simulations with a NPT ensemble (T = 300 K, P = 1 atm) was applied for a total simulation time of 2 nanoseconds. 2) Geometry optimization of the complete simulation box. The resulting supramolecular structure was then analysed, see Figure SI16.2. The density distribution of the different atoms is displayed in Figure SI16.3.

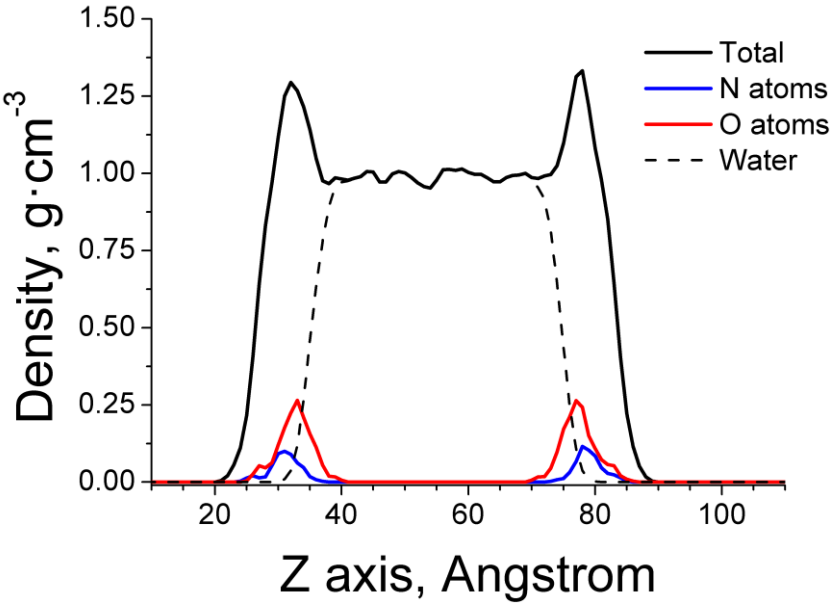

Figure SI16.3. Atomic density distribution of different atom groups as noted in the inset along the z axis. O atoms refer exclusively to those atoms from Fmoc-FF.

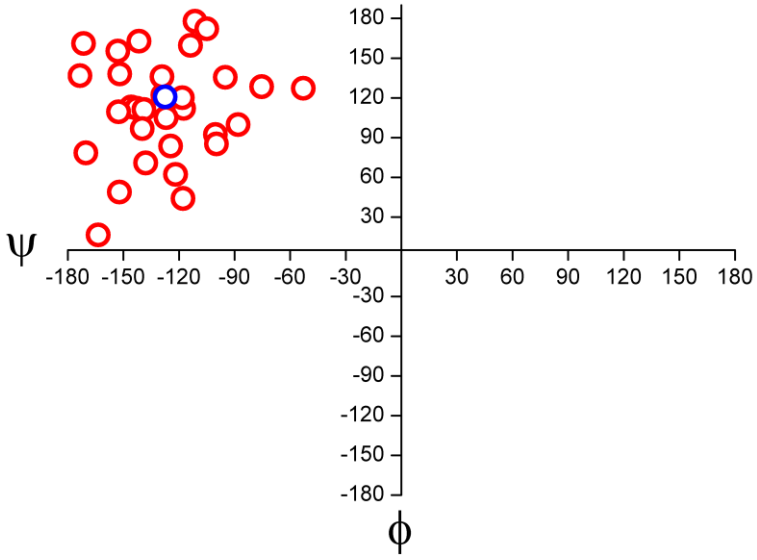

Figure SI16.4. Ramachandran plot for the Fmoc-FF molecules. Red circles: individual measurements for the Fmoc-FF molecules. Blue circle: Average values of the Fmoc-FF molecules for the complete simulation box.

The presence of β-sheet and polyproline II-like features has been obtained in the Ramachandran plot, see Figure SI16.4.[10] The polyproline II-like conformation is obtained from the values of ϕ,ψ angles in the range ϕ,ψ = (-100° to 0°, 100° to 180°). The β-sheet conformation is obtained from values of ϕ,ψ angles in the range ϕ,ψ = (-180° to -100°, 100° to 180°). The approximate relative contribution of each structure is ca. 55% of β-sheet conformation and ca. 10% of polyproline II-like conformation. The following criterion was applied to assess the formation and number of H-bonds: The number of hydrogen bonds was determined with a donor-acceptor distance equal or lower than 3.5 Å and an interaction angle equal or lower than 30°.[10] The number of H-bonds between the peptide bonds is 30 for the complete simulated box, including 32 Fmoc-FF molecules. Note that the carbonyl oxygens, as well as the oxygen atoms from the carbamate group are also able to form H-bonds. Thus, the total amount of H-bonds in the simulated box is 60 H-bonds. An average contribution of two H-bonds per Fmoc-FF molecule with neighbour Fmoc-FF molecules is then obtained. Additionally, the total number of H-bonds formed by Fmoc-FF with water molecules is 215. An average of 6.7 H-bonds per Fmoc-FF molecule has been obtained.

Section SI17. Application of the Extended Dipole Model for assessment of the UV-vis reflection spectra.

The UV-vis absorption spectrum of the Fmoc-FF dipeptide recorded in bulk solution has been deconvoluted onto Gaussian peaks, see Figure SI17.1. The UV-vis reflection spectrum is included for comparison. Please note that alternative deconvolution of the UV-vis band might be used. Therefore, the conclusions of this section should be taken as qualitative.

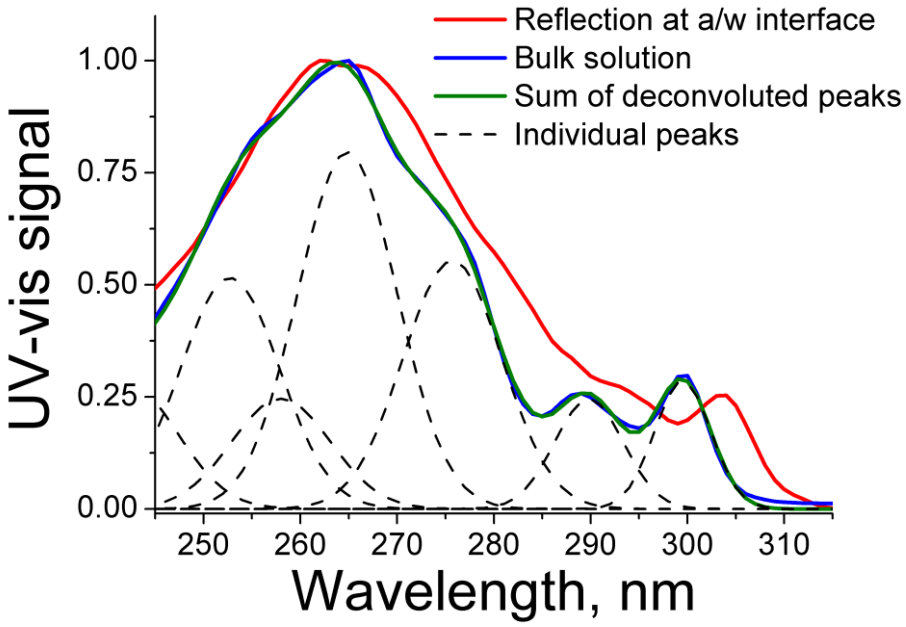

Figure SI17.1. UV-vis reflection spectra of Fmoc-FF molecule, recorded at 0.55 nm^2 per Fmoc-FF molecule (red line). UV-vis absorption spectrum of Fmoc-FF molecule recorded in bulk solution (blue line). Deconvolution of the spectrum onto individual peaks (dashed line) and the sum of the individual peaks (green line).

The UV-vis bands for $\lambda > 235$ nm might be deconvoluted onto 7 absorption modes, see Figure SI17.1. The 7 absorption modes arise from the absorption of the Fmoc group. However, the vertical transitions obtained with standard TD-DFT calculations did not lead to a general agreement with the observed spectral features for the Fmoc group.[2] The quantum calculations using TD-B3LYP/6-31+G(d,p) render only three transitions. Such transitions are: 276 nm (B_2 symmetry and oscillator strength f = 0.17), 265 nm (B2 symmetry and oscillator strength f = 0.29) and 256 nm (A_1 symmetry and oscillator strength f = 0.01). These three transitions are related to the following peaks: 276 nm, 265 nm and 258 nm, see Figure SI17.1. The peaks observed at a 253 nm and 242 nm with B_2 symmetry might be related with the excited vibrational modes at 276 and 265 nm. The bands at 299 nm and 290 nm cannot be clearly ascribed to a set of transitions. These peaks have been related with the excited state geometry rearrangements, leading to substantial differences between vertical and adiabatic transitions energies, as well as vibronic

coupling phenomena, indicating partial breakdown of the Born–Oppenheimer approximation. These peaks also display B_2 symmetry.[11]

The shift of the UV-vis reflection spectra when compared to the UV-vis absorption spectrum in bulk solution towards longer wavelength values might be quantitatively assessed by applying the extended dipole model.[12–14] In the frame of the extended dipole model, all absorption modes in the Fmoc group are replaced by their transition dipoles, $\mu_i = \ell_i \times q_i$, with fixed dipole length (ℓ_i) and charge (q_i). Given a Fmoc group as a reference molecule and an absorption mode i, the interaction of the Fmoc reference molecule with all the dipoles j form the neighbour Fmoc molecules might be considered for obtaining the exciton interaction from the aggregation of the Fmoc molecules. As a common assumption, the interaction of the i component with the i component of the neighbour Fmoc molecule (Fmoc number 2) is exclusively considered. This assumption is valid unless the difference between the energy values for the absorption transitions between the modes i and j is not significant compared with the energy of interaction between the dipoles.[15]

Given a Fmoc reference molecule (Fmoc number 1), the average excitation energy of this reference molecule, at the i absorption mode selected and due to the aggregation with N neighbor molecules can be expressed as:

$$\Delta E_{1,N} = \Delta E_{mon} + 2\sum_{k=2}^{N} J_{1,k}\,\frac{2\left(N+1-k\right)}{N}$$

ΔE_{mon} is the excitation energy of the monomer, N is the aggregation number, being k = 2, 3, … N, and $J_{1,k}$ is the interaction energy between the dipoles of the 1 and k molecules, corresponding at the i absorption mode selected, which can be expressed in an approximately way by

$$J_{1,\mathrm{k}} = \frac{q_i^2}{D}\left[\frac{1}{ac_{1,\mathrm{k}}} + \frac{1}{bd_{1,\mathrm{k}}} - \frac{1}{ad_{1,\mathrm{k}}} - \frac{1}{bc_{1,\mathrm{k}}}\right]$$

with D of ca. 2.7 is the dielectric constant, and ac, bd, ad and bc are the distances between ends of the dipoles positive–positive, negative–negative, positive–negative and negative–positive, respectively. Thus, the maximum wavelength of the aggregate at the i absortion mode λ_N, is:

$$\lambda_{i,N} = \frac{\lambda_{mon} hc10^7}{hc10^7 + 4\lambda_{mon}\sum_{j=k}^{N} J_{1,\mathrm{k}}\,\frac{\left(N+1-k\right)}{N}}$$

The transition dipole components (μ_i) could be calculated from the band decomposition, but the dipole length (ℓ_i) cannot be obtained from the experimental data. The dipole length value is approximately 66% of the extent of the π conjugate system. A dipole length of $\ell_L \approx 4$ Å is used for all the B_2 symmetry components (long axis transition dipoles), while for the A1 symmetry component (short axis transition dipoles), a dipole length $\ell_S \approx 2$ Å is used, see Figure SI17.2.[16]

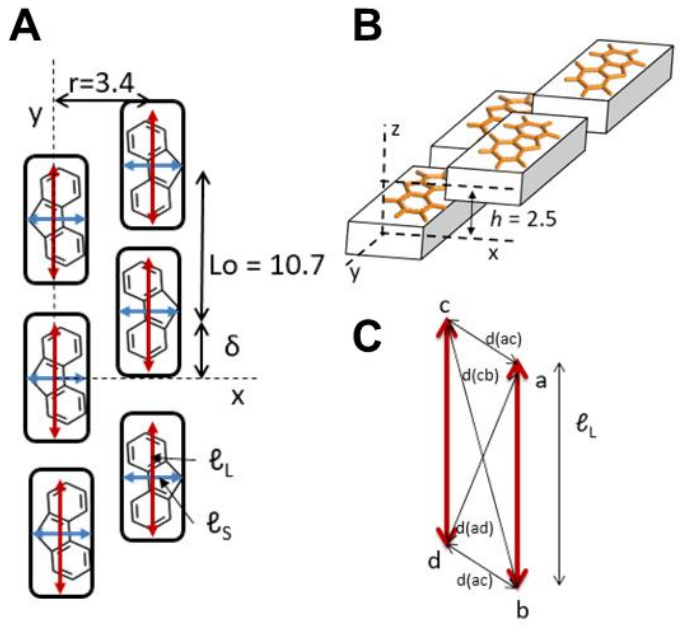

Figure SI17.2. Molecular sketches for the application of the Extended Dipole Model to the Fmoc-FF supramolecular structure.

Lineal aggregates with infinite length of Fmoc-FF molecules are assumed to be formed at the air/water interface (N = ∞). The relative arrangement of two consecutive molecules is set from the final snapshot of the molecular dynamics simulations. Neighbour Fmoc-FF molecules are assumed to be distributed among approximately two parallel rows with a relative displacement δ, see FigureSI17.2A. Such rows are distributed along the y axis, being L_0 the separation between molecules of the same row, r, the distance between rows along the x axis, and h, the displacement between the rows along the z axis, see FigureSI17.2.

Three absorption components of the Fmoc-FF molecule are analysed using the extended dipole model as displayed in Figure SI17.3. The values of shift of wavelength for the absorption modes at 265 nm and 299 nm (B_2 symmetry) and the absorption mode at 258 nm (A_1 symmetry) are shown in Figure SI15.3. The bands with B_2 symmetry are shifted towards longer wavelength, corresponding to the formation of J-aggregates. The absolute value of the shift of the spectrum is a function of the maximum value of wavelength of the band and the value of the transition dipole. Using 2.5 D and 1.75 D for the dipole transition for the bands at 265 nm and 299 nm, the shift of the band shows a slight dependence with the relative displacement (δ) up to 6 nm and 4 nm, respectively.

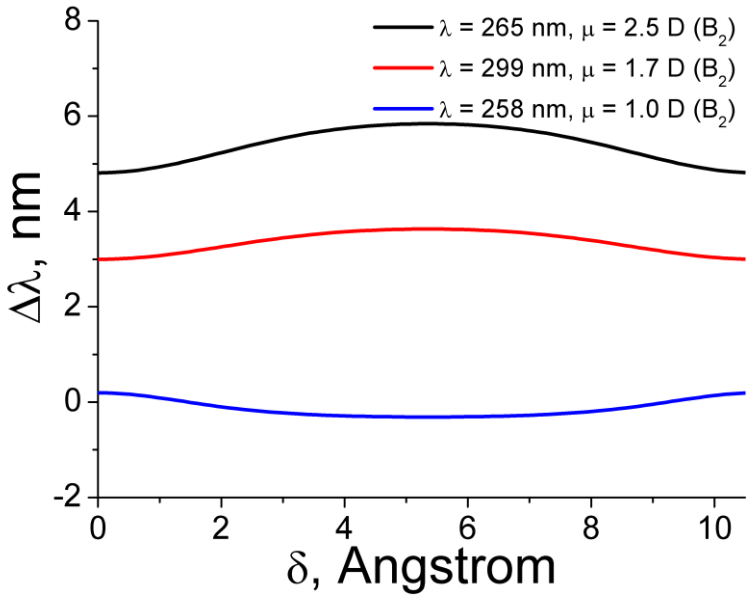

Figure SI17.3. Calculated values for shift of wavelength for the three absorption modes of Fmoc-FF dipeptide as a function of relative molecular displacement (δ).

The band with A_1 symmetry might be shifted towards shorter or longer wavelength depending on the relative molecular displacement (δ). Note that in all cases such shift on the wavelength is rather reduced, smaller than 1 nm. A dipole transition of 1 D is used, obtained from the value of the oscillator strength f = 0.01.[2] The modification of the morphology of the bands when comparing the UV-vis reflection spectra at the air/water interface with the UV-vis absorbance spectrum in bulk solution for the Fmoc-FF dipeptide is related with the different shift of peaks with B_2 and A_1 symmetry. The peaks with B_2 symmetry exhibit a shift towards longer wavelength from 4 to 6 nm, whereas no significant shift is observed for the peaks with A1 symmetry.

This significant difference on the interaction between UV-vis bands as a function of their symmetry is checked by introducing a shift of 4 to 7 nm to the bands with B_2 symmetry, whereas the A_1 peak at 262 nm is not shifted. The height of the peaks might be slightly modified, although the area of the peaks is kept constant in all cases, see Figure SI17.4.

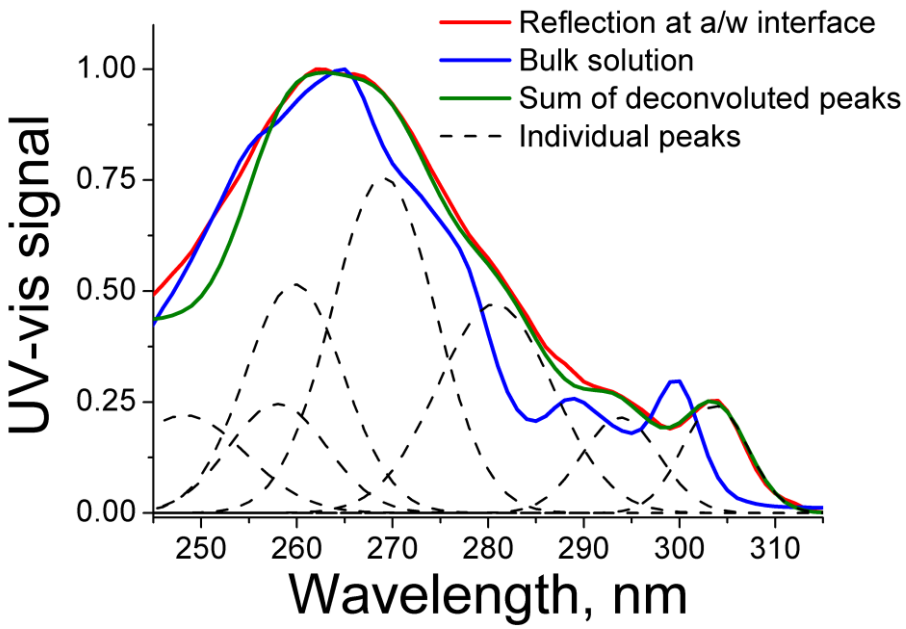

Figure SI17.4. UV-vis reflection spectra of Fmoc-FF molecule, recorded at 0.55 nm^2 per Fmoc-FF molecule (red line). UV-vis absorption spectrum of Fmoc-FF recorded in bulk solution (blue line). Deconvolution of the spectrum onto individual peaks (dashed line) and the sum of the individual peaks (green line). A shift of 4-7 nm is included for the bands with B_2 symmetry.

Remarkably, the sum of the deconvoluted peaks is almost coincident with UV-vis reflection spectrum of the Fmoc-FF at the air/water interface. Additionally, the maximum of the band is shifted towards shorter wavelength, despite the opposite shift of the B_2 bands towards longer wavelength. The A_1 band and the band at 254 nm (bulk solution) that is shifted 7 nm (air/water interface) are placed at the same wavelength, then placing the maximum at 262 nm. This behaviour might explain the experimentally observed shifts in the UV-vis spectra.

The Fmoc-CF shows no modification of the morphology of the bands, instead displaying a net shift of all the peaks towards shorter wavelength. This phenomenon might be ascribed to different values of the orientation factor f. As example values, f lower than 1 for the A_1 bands and f = 1.5 for the B_2 bands would render to the observed shift of the entire UV-vis spectrum for the Fmoc-CF. Note that the circular dichroism spectra in the region of 260 nm of Fmoc-CF shows significant differences with respect to the Fmoc-FF, thus pointing to conformational changes that would support the mentioned variation in the orientation factor values.

REFERENCES

(1) Kaiser, E.; Colescott, R. L.; Bossinger, C. D.; Cook, P. I. *Anal. Biochem.* **1970**, *34* (2), 595.

(2) Nguyen, D. D.; Trunk, J.; Nakhimovsky, L.; Spanget-Larsen, J. *J. Mol. Spectrosc.* **2010**, *264* (1), 19.

(3) Zou, Y.; Razmkhah, K.; Chmel, N. P.; Hamley, I. W.; Rodger, A. *RSC Adv.* **2013**, *3* (27), 10854.

(4) Zhang, Y.; Gu, H.; Yang, Z.; Xu, B. *J. Am. Chem. Soc.* **2003**, *125* (45), 13680.

(5) Smith, A. M.; Williams, R. J.; Tang, C.; Coppo, P.; Collins, R. F.; Turner, M. L.; Saiani, A.; Ulijn, R. V. *Adv. Mater.* **2008**, *20* (1), 37.

(6) Eckes, K. M.; Mu, X.; Ruehle, M. A.; Ren, P.; Suggs, L. J. *Langmuir* **2014**, *30* (18), 5287.

(7) Chemicalize https://chemicalize.com/ (accessed Sept 10, 2018).

(8) Rappe, A. K.; Casewit, C. J.; Colwell, K. S.; Goddard, W. A.; Skiff, W. M. *J. Am. Chem. Soc.* **1992**, *114* (25), 10024.

(9) Gasteiger, J.; Marsili, M. *Tetrahedron* **1980**, *36* (22), 3219.

(10) Mu, X.; Eckes, K. M.; Nguyen, M. M.; Suggs, L. J.; Ren, P. *Biomacromolecules* **2012**, *13* (11), 3562.

(11) Bree, A.; Zwarich, R. *J. Chem. Phys.* **1969**, *51* (3), 903.

(12) Czikkely, V.; Försterling, H. D.; Kuhn, H. *Chem. Phys. Lett.* **1970**, *6* (1), 11.

(13) Czikklely, V.; Forsterling, H. D.; Kuhn, H. *Chem. Phys. Lett.* **1970**, *6* (3), 207.

(14) Giner-Casares, J. J.; De Miguel, G.; Pérez-Morales, M.; Martín-Romero, M. T. M. T.; Camacho, L.; Muñoz, E. *J. Phys. Chem. C* **2009**, *113* (14), 5711.

(15) Parson, W. W. Springer-Verlag: Berlin, 2007.

(16) Kuhn, H.; Kuhn, C. In *J-Aggregates*; Kobayasho, T., Ed.; World Scientific: Singapore, 1996.